Cell-specific Imd-NFκB responses enable simultaneous antibacterial immunity and intestinal epithelial cell shedding upon bacterial infection

Zongzhao Zhai[1, 2] *, Jean-Philippe Boquete[1] and Bruno Lemaitre[1]*

[1]Global Health Institute, School of Life Sciences, Ecole Polytechnique Fédérale de Lausanne (EPFL), Station 19, 1015 Lausanne, Switzerland

[2]Animal Nutrition and Human Health Laboratory, School of Life Sciences, Hunan Normal University, 410081 Changsha, Hunan, China

*Authors for correspondence:

zongzhao.zhai@foxmail.com (Z.Z.)

bruno.lemaitre@epfl.ch (B.L.)[#]

[#] Lead Contact

SUMMARY

Intestinal infection triggers potent immune responses to combat pathogens and concomitantly drives epithelial renewal to maintain barrier integrity. Current models propose that epithelial renewal is primarily driven by damage caused by reactive oxygen species (ROS). Here we found that in *Drosophila*, the Imd-NFκB pathway controlled enterocyte (EC) shedding upon infection, via a mechanism independent of ROS-associated apoptosis. Mechanistically, the Imd pathway synergized with JNK signaling to induce epithelial cell shedding specifically in the context of bacterial infection, requiring also the reduced expression of the transcription factor GATAe. Furthermore, cell-specific NFκB responses enabled simultaneous production of antimicrobial peptides (AMP) and epithelial shedding in different EC populations. Thus, the Imd-NFκB pathway is central to the intestinal antibacterial response by mediating both AMP production and the maintenance of barrier integrity. Considering the similarities between *Drosophila* Imd signaling and mammalian TNFR pathway, our findings suggest the existence of an evolutionarily conserved genetic program in immunity-induced epithelial shedding.

KEYWORDS

Imd-NFκB signaling, innate immunity, enterocyte shedding, enteric infection, enhancer, JNK, *GATAe*, *Drosophila*

INTRODUCTION

Epithelial tissues such as the skin and the epithelial linings of the digestive tract form dynamic barriers between the body and the external environment. They perform diverse physiological functions while fending off constant challenge from a variety of factors including microorganisms. Damaged epithelial cells are shed from the epithelium and rapidly replenished to maintain tissue integrity through the action of stem cells. Stem cell proliferation and differentiation are tightly adjusted to compensate for the number of cells lost, so as to maintain an internal steady state known as tissue homeostasis (Blanpain and Fuchs, 2014). Recent studies have uncovered the complex mechanisms underlying stem cell activation and maintenance of tissue homeostasis, notably through feed-back signals sent from stressed epithelial cells to stem cells to promote their proliferation (Barker, 2014; Guo et al., 2016; Jiang and Edgar, 2012). While research has mostly focused on stem cells, epithelial cell shedding constitutes an integral part of epithelial turnover (Patterson and Watson, 2017; Vereecke et al., 2011). Aberrant epithelial cell shedding can lead to unsealed breaches and underlies inflammatory bowel diseases. However, the genetic program that epithelial cells use to sense damage and delaminate into the gut lumen is not well understood.

Research in *Drosophila* has provided insights into the maintenance of intestinal homeostasis and epithelial immunity (Buchon et al., 2013a; Guo et al., 2016). In the adult *Drosophila* midgut, intestinal stem cells (ISCs) differentiate into either polyploid absorptive enterocytes (ECs) or diploid secretory enteroendocrine cells (EEs). Differentiating ISC daughter cells called enteroblasts (EBs) are precursors of ECs, and ISCs and EBs are collectively referred to as midgut progenitors. In *Drosophila*, enteric infection rapidly leads to EC death through shedding into the gut

lumen (Buchon et al., 2010). Infection-induced EC death in *Drosophila* is so far largely attributed to the production of reactive oxygen species (ROS) by the *Drosophila* NADPH Dual Oxidase (Duox). While ROS neutralize invading microbes, they are also believed to damage ECs leading to their elimination (Buchon et al., 2009a; Lee et al., 2013).

In addition to triggering ROS production, enteric infection also activates the immune deficiency (Imd) pathway in the *Drosophila* gut (Buchon et al., 2013a). This pathway regulates the transcription of genes encoding antimicrobial peptides (AMPs) in the gut during ingestion of pathogenic bacteria or in response to beneficial gut microbiota. Imd signaling is triggered by the recognition of diaminopimelic acid (DAP)-type peptidoglycan, a component of the cell wall of Gram-negative bacteria and *Bacillus* species. Peptidoglycan sensing is mediated through the surface-bound pattern recognition receptor PGRP-LC or the cytosolic receptor PGRP-LE. Activation of these receptors initiates a complex signaling cascade, involving the adaptor protein Imd, the caspase 8-like protease Dredd, the E3 ubiquitin ligase Diap2, the MAPKK kinase dTAK1 and the IKK complex and eventually leads to the activation and cleavage of the NFκB-like transcription factor Relish (Rel) (Kleino and Silverman, 2014). The N-terminal part of Relish then translocates into the nucleus to induce the transcription of genes coding AMPs (*e.g. Diptericin* (*Dpt*)) and negative regulators of the pathway including *pirk* and the amidase *PGRP-LB*.

Transcriptomic analyses have revealed that the Imd pathway regulates not only the production of AMPs in the gut, but also genes not associated with immune functions (Broderick et al., 2014; Buchon et al., 2009b; Erkosar et al., 2014), suggesting that this pathway executes non-immune programs (reviewed in Zhai et al., 2017b). Indeed, Imd signaling is implicated in apoptosis (Georgel et al., 2001), and

some of the Imd components have been implicated in cell death in non-immune contexts, such as eliminating unfit cells during cell competition (Meyer et al., 2014) and neuronal cell death (Petersen et al., 2012). In the adult *Drosophila* midgut, increased Imd activity upon infection (Buchon et al., 2009b; Jiang et al., 2009) or upon loss of negative regulators (Mistry et al., 2017; Paredes et al., 2011; Ryu et al., 2008) is also associated with cell death. Yet, the molecular mechanisms linking elevated Imd immune signaling to cell death in the intestinal epithelium are not known.

Here we found that the Imd pathway controlled EC shedding upon bacterial infection. By analyzing the cis-regulatory sequence of the *unpaired 2* (*upd2*) gene, we identified an enhancer sequence that was turned on specifically in damaged ECs upon bacterial infection. This sequence harbored an NFκB motif and could be used as a marker to visualize shedding ECs. Using this reporter, we found that the Imd pathway was not only involved in the antibacterial immune response but also contributed to EC shedding upon enteric infection. EC shedding upon bacterial infection required both the Imd and JNK pathways and was negatively regulated by the GATAe transcription factor. Thus, the Imd pathway enables a dual response to infection via both promoting the production of AMPs and through regulating epithelial cell shedding to ensure appropriate epithelial turnover and the maintenance of barrier integrity during infection.

RESULTS

An Infection-Inducible Enhancer of *upd2* Marks Delaminating ECs

Enteric infection with the Gram-negative bacterium *Erwinia carotovora carotovora 15* (*Ecc15*) increases the rate of intestinal epithelial renewal in *Drosophila*, a process that involves the shedding of ECs and the production of new epithelial cells by resident stem cells (Buchon et al., 2010). Intestinal homeostasis is maintained by a feedback loop in which damaged ECs promote stem cells to divide and differentiate through the release of secreted factors. Notably, secretion of the Upd2 and Upd3 non-cell-autonomously activate the JAK-STAT pathway to stimulate stem cells by binding to the cell surface receptor Domeless (Dome), a homolog of JAK receptors, in the neighboring ISC and EBs (Buchon et al., 2009b; Jiang et al., 2009) (**Fig 1A**). We hypothesized that cis-regulatory elements of these *Upd* genes harbor a combination of binding sites for transcription factors activated upon damage. To better understand the damage-sensing program involved in EC shedding, we systematically surveyed the regulatory sequences over a 6 kilobase pair (kb) region upstream of the *upd2* coding sequences (**Fig 1B**). Transgenic reporter lines were generated to study the enhancer activities of these fragments *in vivo* under both basal (i.e. unchallenged) conditions and oral infection with *Ecc15*. Two DNA fragments (*upd2_A* and *upd2_B*) showed enhancer activity in midgut progenitors, while the *upd2_D* sequences drove reporter expression in a subset of EEs in the middle midgut, under both conditions. We also identified a 1kb region, *upd2_C*, which conferred inducible reporter expression. The *upd2_C* reporter gene showed almost no expression under basal conditions but was strongly induced in ECs after oral infection with *Ecc15* (**Fig S1A**). A 498bp sub-region of *upd2_C*, the *CB* fragment, recapitulated the expression profile of *upd2_C*. Further dissection of the *CB* enhancer allowed us to identify a 204bp fragment that we named *CBM* (*CB* minimal enhancer), which completely recapitulated the enhancer activity of the *CB* fragment (**Fig S1B**).

In contrast, a GFP reporter driven by three other sub-fragments of *upd2_CB* (*CB_S1-3*) did not show any expression in both conditions. Examination of the *CBM* sequences revealed the presence of conserved binding sites for the JNK transcription factors AP1 (TGANTCA), GATA factor (GATAR) and homeobox protein (TTATT or TAATT) (**Fig 1B and S1C**). The *CBM* fragment also harbored an NFκB motif (GGGRNYYYYY), which is usually found in the regulatory DNAs of immune responsive genes.

The midgut of 4-10-day-old adult flies carrying one copy of *CB* transgenic reporter was formed by a mono-layered epithelium with few dying cells occasionally found in the gut lumen (**Fig 1C**). Oral infection of flies with *Ecc15* caused massive EC shedding starting from 4 hours post infection (**Fig S1D**). Dying ECs present in the gut lumen became easily detectable at 8-12 hours post infection (**Fig 1D**). The EC identity of the delaminating cells was confirmed by their large nuclear size, apical localization, expression of EC maker *Myo1A>GFP* and absence of the progenitor marker *esg::GFP* (**Fig 1D-E and S1E**). Nearly all the ECs at the early stages of detaching from the epithelium expressed the *CB-mCherry* reporter (**Fig 1E**), indicating that the *CB* enhancer is specifically activated in shedding ECs. However, ECs that had been shed into the gut lumen did not appear to consistently maintain *CB-mCherry* expression. The dynamic reporter expression in shedding and/or shed ECs was further supported by quantitative measurements of *CB* reporter levels in ECs according to their basal to luminal positions (**Fig S1F**). Analyses of nuclear morphology revealed that ECs detached from the epithelium without any sign of apoptosis, but underwent cell death at a later step of shedding in the lumen (orange arrows, Fig 1E and S1E). Shed ECs displayed classic apoptotic features, including the ring or necklace-shaped chromatin condensation (white arrows, Fig 1E and S1E)

followed by nuclear collapse and disassembly (yellow arrows, Fig 1E and S1E) (Tone et al., 2007). EC shedding as revealed by the induction of the *CB>CD8GFP* reporter was more prominent in the posterior midgut ($R4_{bc}$ according to Buchon et al., 2013b) and was associated with a strong contraction of the visceral muscle (**Fig S1G**). Thus, *upd2_CB* provides a valid marker of shedding ECs as well as a tool to uncover the genetic program leading to EC shedding. In the next sections of the paper, we used the *CB* reporter to visualize EC shedding. However, it is important to note that *upd2* itself is not required for the EC shedding process. In fact, the JAK-STAT receptor and therefore the pathway activity is restricted to progenitors, excluding a role of this pathway in ECs.

The *upd2_CB* Enhancer is Specifically Activated by Gram-negative Bacteria

Oral infection with *Ecc15* activates the Imd pathway (**Fig 2A**) as well as the production of ROS through the activity of the NADPH oxidase Duox (*Dual oxidase*). A series of experiments demonstrated that the *CB* element was not activated by ROS but by determinants associated with Gram-negative bacteria. Oral infection with the uracil-deficient *Ecc15* strain, which does not activate Duox (Lee et al., 2013), still activated the *CB>CD8GFP* reporter to the same extent as a wild-type strain of *Ecc15* (**Fig 2B-C**). In addition, RNAi of *Duox* in ECs did not attenuate *Ecc15* infection-induced Imd activation, *CB-mCherry* reporter expression or EC shedding (**Fig S2A-B**). Moreover, the *CB* element was also induced by a derivative of the Gram-negative bacterium *Pseudomonas entomophila*, *P. entomophila gacA*, which is completely avirulent but retains the capacity to trigger Imd signaling (Liehl et al., 2006) (**Fig S2C**). In contrast, ingestion of either a Gram-positive bacterium, *Micrococcus luteus* for 12 hours (Neyen et al., 2014) or 10% dextran sulfate sodium (10% DSS), a corrosive agent that damages the intestine (Amcheslavsky et al., 2009), for 36 hours

did not activate the reporter (**Fig 2D-E**). Oral infection with the Gram-negative *Serratia marcescens* Db11 strain, which causes thinning of the gut epithelium without inducing EC death or Imd activity (Lee et al., 2016), failed to induce *CB* reporter expression (**Fig S2D**). Collectively, these data suggest that *CB* reporter expression in delaminating ECs is specifically induced by determinants associated with Gram-negative bacteria and activation of the Imd pathway.

The *CB* Reporter is Regulated by the NFκB-like Transcription Factor Relish

We next investigated whether the Imd pathway regulates the *CB* reporter. This pathway can be activated by oral bacterial infection or by over-expressing *PGRP-LC* in ECs. RNAi depletion of *Relish* or *Dredd* in ECs of *Ecc15*-infected flies reduced the expression of the antibacterial gene *Dpt*, a read-out of the Imd pathway, as expected. Loss of *Relish* or *Dredd* also abolished the expression of the *CB-mCherry* reporter. In contrast, the activation of the widely used *upd3* reporter, *upd3.1-lacZ* (Jiang et al., 2011), which is known to respond to epithelial damage, was not affected (**Fig 2F and S2E-F**). Activation of the Imd pathway by over-expressing *PGRP-LCx* in ECs was sufficient to activate both *Dpt* and the *CB-mCherry* reporter, and their expression required the Imd pathway components Relish, Imd, Dredd or TAK1 (**Fig 2G and S2G-I**). Thus, induction of the *CB-mCherry* reporter upon bacterial infection requires the Imd pathway.

We then tested whether the *CB* enhancer is directly regulated by the NFκB-like factor Relish. To this aim, we expressed two transcriptionally active forms of Relish, *Rel-VP16* and *RelD*, in ECs and then examined the activation of *CB-mCherry*. *Rel-VP16,* a strong activator of Imd signaling, is a fusion of the VP16 activation domain to the *N*-terminal of the full-length Relish protein, while *RelD*, a weak activator of Imd signaling, is the *N*-terminal DNA binding domain of Relish without

the inhibitory ankyrin region (DiAngelo et al., 2009). Expressing *RelD* mildly activated *CB-mCherry* as well as *Dpt, pirk* and *PGRP-LB,* while expressing *Rel-VP16* for three days led to a 130-fold induction of the *CB-mCherry* reporter, a level significantly higher than that achieved by over-expressing *PGRP-LCx* (**Fig 2H-K**). Of note, although Rel-VP16 greatly activated the *CB-mCherry* reporter and the negative regulators *pirk* and *PGRP-LB,* it did not increase the expression of *Dpt* (**Fig 2K**). This is in line with the notion that AMP gene expression requires not only the Imd pathway but also additional cell type-specific transcriptional factors (Zhai et al., 2017b).

Consistent with a direct regulation of the *CB* element by Relish, a mutated version of the *CB* reporter, *CB.mtNFκB-mCherry,* in which the NFκB site was abolished, was not activated upon *Ecc15* infection, despite the presence of many delaminating cells in the gut lumen (**Fig 2L-N**). Moreover, *CB.mtNFκB-mCherry* was not induced by over-expressing *Rel-VP16* or *RelD* in ECs (**Fig 2O**). This indicates that the *CB* fragment of the *upd2* gene is a target of Relish downstream of the Imd pathway.

Distinct Expression Pattern of *Dpt* and *CB* Reporters along the Gut

Having shown that the *CB-mCherry* reporter was a target of Imd signaling, we next tested the range of cell types along the gut that are responsive to Imd activation. For this, we applied mosaic analysis with the *esgF/O* system (Jiang et al., 2009) to generate GFP-labeled clones of cells that contained both progenitors and their differentiated progenies that over-expressed *PGRP-LCx* or *Rel-VP16* (**Fig 3A**). Only ECs within the GFP-positive clones expressed the *CB-mCherry* reporter, indicating a cell-autonomous activation by the Imd pathway restricted to ECs (**Fig 3B and S3A-C**). Similarly, the Imd-responsive *Dpt* reporters (*Dpt-lacZ* or *Dpt-mCherry*) were also

exclusively induced in ECs (**Fig 3C and S3D**). These results suggest that ECs are the primary Imd-responsive cell type in the *Drosophila* midgut.

The adult midgut is a compartmentalized organ showing differences in morphology, stem cell activity, metabolic, and digestive function along its length (Buchon et al., 2013b; Marianes and Spradling, 2013). We found that the *CB* and *Dpt* reporters were expressed in a non-overlapping and nearly complementary manner (**Fig 3D, 3F and S3E-F**). While strong *CB* reporter (*CB>CD8GFP* or *CB-mCherry*) expression was found at regions $R2_{bc}$, R3 and $R4_{bc}$ (midgut regions according to Buchon et al., 2013b), the *Dpt* reporter gene was induced at regions R0, R1, $R2_a$, B_{R2-R3}, B_{R3-R4} and $R4_a$, that did not show EC shedding upon *Ecc15* infection (**Fig 3E**). *Dpt* expression was mostly observed in gut domains with limited radius and reduced lumen size, notably the two constrictions B_{R2-R3} and B_{R3-R4} that surround the copper cell region in the middle midgut. We speculated that production of AMPs in these bottlenecks can maximize the effectiveness of AMPs in neutralizing invading bacteria. On the other hand, strong *CB* reporter expression coincided with regions showing higher epithelial renewal rate except R3 (Marianes and Spradling, 2013). We conclude that AMP production and EC shedding as revealed by the *Dpt* and *CB* reporters, two different gut responses to infection, take place in distinct gut regions.

Bacterial Infection-induced EC Shedding Requires the Imd Pathway

The observation that the *CB* reporter, a marker of shedding ECs, was regulated by the Imd pathway prompted us to investigate whether the Imd pathway is required for EC shedding. Midguts from Rel^{E20} or $Dredd^{B118}$ flies did not exhibit delaminating ECs upon infection with *Ecc15* (**Fig 4A-D, G**). Expressing a full-length *Relish* in the ECs of Rel^{E20} flies restored the ability of ECs to delaminate upon infection (**Fig S2J-K**). Previous studies have shown that the Imd pathway is activated in the midgut by

the intracellular receptor PGRP-LE but not PGRP-LC (Bosco-Drayon et al., 2012; Neyen et al., 2012). Consistent with a role of the Imd pathway in EC shedding, *PGRP-LE* but not *PGRP-LC* was found to be necessary for infection-induced EC shedding (**Fig 4E-G**). We conclude that beyond its well-established role in AMP production, the Imd pathway is also required for EC shedding upon infection.

We then investigated whether Imd activation is sufficient to trigger EC shedding. Consistent with this, over-expressing *PGRP-LCx* or Relish-VP16 using the EC-specific driver, $Myo1A^{TS}$, induced massive EC shedding into the gut lumen **(Fig 4H-I and S2G-H)**. We next generated mosaic clones using the *esgF/O* system, to study whether EC shedding is cell-autonomously activated by Imd signaling. Confocal sections revealed that many *CB-mCherry* expressing ECs that over-expressed *PGRP-LCx* were extruding apically into the gut lumen. This phenotype was cell-autonomous as neither their wild-type neighbors nor GFP-marked wild-type ECs displayed the same migratory behavior (**Fig 4J-K**). Furthermore, activation of the effector caspase, Caspase 3, was observed in the midgut of wild-type but not *Relish* mutant flies upon infection **(Fig 4L-N),** suggesting that EC detachment precedes activation of the apoptotic machinery. Collectively, this indicates that the Imd pathway controls EC shedding into the gut lumen upon bacterial infection. As such, the Imd pathway represents a *bona fide* cell elimination pathway.

ISC Proliferation upon Bacterial Infection does not Require the Imd Pathway

It is generally assumed that ISC proliferation is coupled to EC elimination through feedback mechanisms, notably through the production of secreted factors (e.g. Upd2 and Upd3) activating stem cells during regeneration (Buchon et al., 2009b; Jiang et al., 2009; Liang et al., 2017). According to this notion, *Relish* flies should exhibit reduced ISC proliferation upon infection, as ECs did not delaminate in this

mutant. However, we did not detect any difference in the mitotic index at 10 hours post infection between the w^{1118} control and Rel^{E20} mutant flies (**Fig 5A**), in agreement with a previous study (Buchon et al., 2009b). Consistent with this, qPCR showed that *upd2* and *upd3* were induced to the same level in the midgut of *Relish* and wild-type flies upon infection (**Fig 5B**). The induction of *upd2* in *Relish* flies was at first sight surprising, considering our data showing that the *CB* enhancer of *upd2* was activated in a *Relish*-dependent manner in ECs. We reasoned that since *upd2* is also expressed in midgut progenitors (Zhai et al., 2015), changes of *upd2* expression in ECs could have been masked when assayed in whole midgut extracts. Further qPCR measurements using FACS-sorted ECs confirmed that *upd2* but not *upd3* was less induced in ECs of Rel^{E20} flies upon infection (**Fig 5C**). We conclude that Relish is required for EC shedding and *upd2* expression in ECs upon infection, but that Relish does not affect ISC proliferation. Thus, the processes of EC delamination and ISC proliferation can be regulated independently.

Relish is Specifically Required for Bacterial Infection-induced EC Death

We then examined whether *Relish* is required for other forms of EC death that are not linked to an infection. EC death can be triggered by expressing i) the proapoptotic gene *reaper* (*rpr*), or ii) a constitutively active form of the JNK kinase *hemipterous* (hep^{CA}) (Jiang et al., 2009). These manipulations significantly increased the expression of *CB-mCherry* and *upd3.1-lacZ* reporters, and *upd2* and *upd3* endogenous genes, but did not prominently induce the expression of *Dpt* (**Fig S4A**). This indicates that very strong JNK activation can overcome the requirement of the Imd pathway to induce *CB* reporter expression. Expressing *reaper* rapidly induced massive EC apoptosis and resulted in a much-shortened midgut. However, this phenotype was not blocked in Rel^{E20} flies (**Fig S4B**). Similarly, over-expressing either

reaper or *hep*^{CA} led to the same level of EC delamination, ISC proliferation, and expression of *upd2*, *upd3*, *keren* (encoding one of the EGFR ligands) and the JNK target gene *puckered* (*puc*), in wild-type and *Relish* mutant flies (**Fig 5D and S4C**). In sharp contrast, increased ISC proliferation caused by over-expressing *PGRP-LCx* was completely dependent on *Relish* (**Fig 5D**). ISC tumors induced by the loss of Notch also cause EC shedding (Patel et al., 2015). Despite the fact that *CB-mCherry* was induced in the detaching ECs (**Fig S4D**), *Notch* tumor-induced EC death and proliferation of the tumor cells was not inhibited in *Rel*^{E20} flies (**Fig 5E and S4E**). Taken together, these data show that *Relish* is exclusively required for EC death triggered by bacterial infection but not by other abiotic stresses. The observations that *CB-mCherry* was strongly induced by JNK activation via expressing *hep*^{CA} **(Fig S4A)**, and that ISC tumors that lead to JNK activation in surrounding ECs (Patel et al., 2015) also induced *CB-mCherry* therein, suggest that the *CB* enhancer likely also receives transcriptional input from the JNK pathway, under conditions where the Imd pathway is not activated.

JNK signaling Cooperates with the Imd Pathway to Induce EC shedding during Infection

JNK signaling has been widely implicated in apoptosis and tissue remodeling (Pastor-Pareja et al., 2004; Uhlirova and Bohmann, 2006), as well as EC stress and renewal of the gut epithelium (Biteau et al., 2008; Zhou et al., 2017). The presence of an AP1 site in the *CB* element prompted us to analyze the contribution of JNK activity to the Imd-dependent EC shedding in the context of bacterial infection.

qPCR indicated that the JNK activity reporter gene *puckered* (*puc*) was induced about 2-fold during the course of *Ecc15* infection (**Fig 6A**), albeit to a much lower level than that obtained by over-expressing *hep*^{CA} in ECs, which induced *puc*

expression by 40-fold (compare **Fig 6A** to **S4C**). Using a *puckered* reporter line (*puc^{E69}-Gal4/UAS-GFP*) as a readout for JNK activity (Pastor-Pareja et al., 2004), we found that *CB-mCherry* was induced upon infection in a subset of ECs with high levels of JNK activity (**Fig 6B**). Inhibiting JNK signaling by expressing a dominant negative form of the JNK Basket (*bsk^{DN}*) in ECs significantly reduced the expression of *CB-mCherry* but not *upd3.1-lacZ* reporter (**Fig 6C-D**), and suppressed EC shedding upon *Ecc15* infection (**Fig 6D-E**). However, decreased *CB-mCherry* expression upon JNK inhibition was not accompanied by a significant drop in *Dpt* levels (**Fig 6C**). This indicates that JNK signaling is specifically required in EC shedding but not in AMP production, in contrast to Imd signaling which controls both processes. Furthermore, preventing apoptosis by expressing the baculovirus P35 protein had no effect on the induction of *CB-mCherry*, *upd3.1-lacZ* and *Dpt* (**Fig 6C**), and on EC shedding upon infection (**Fig 6E**). Thus, the classic apoptotic pathway is not essential to prime EC shedding upon infection. This suggests that ECs are most likely extruded alive but undergo apoptosis at a later step in the gut lumen (**Fig 1E and S1E**). Of note, caspase-independent cell shedding also occurs in *C. elegans* embryos and mammalian intestinal epithelium (Coopersmith et al., 1999; Denning et al., 2012).

To assess the role of the JNK pathway in regulating the *CB* element, we generated a transgenic reporter containing the *CBM* element with a mutated AP1 site. While the *CBM.mtAP1-GFP* reporter displayed a basal-level expression similar to its wild-type counterpart, it was not activated upon *Ecc15* infection (**Fig 6F-G**). This confirms that the *CBM* enhancer is directly targeted by the JNK transcription factors through the AP1 site. Strong JNK activation by expressing *hep^{CA}* in ECs for 15 hours induced *CB-mCherry* more than 30-fold but *CB.mtNFκB-mCherry* only 6-fold (**Fig**

6H and S5A-B), indicating that the NFκB binding site can modulate the magnitude of induction in the *CB* element by JNK. This supports the notion that the JNK pathway cooperates with Imd signaling to regulate *CB* reporter expression and EC shedding. This cooperation is, however, not required for the expression of antibacterial genes in the fly intestine.

The Imd pathway bifurcates downstream of TAK1 to activate both JNK signaling and IKK kinase, the latter leading to the activation of Relish (Silverman et al., 2003). However, we found that activation of the JNK pathway in infected ECs was not a direct consequence of Imd activation. First, induction of *puc* and two other JNK targets coding for matrix metalloproteinases (*Mmp1* and *Mmp2*) (Uhlirova and Bohmann, 2006) was not blocked in Rel^{E20} guts during infection (**Fig S5C**). Second, although *TAK1* was absolutely necessary for activation of the Imd pathway, it proved dispensable for induction of JNK signaling in the midgut upon oral infection (**Fig S5D**). Third, JNK activation upon infection was not reduced in *PGRP-LC*, *PGRP-LE* or *imd* mutants **(Fig S5E)**. Fourth, flip-out clones over-expressing *PGRP-LCx* showed *puc-lacZ* expression, but this induction was not cell-autonomous and thus not a direct consequence of *PGRP-LCx* expression (**Fig S5F**). Fifth, increased ISC proliferation induced by over-expressing *PGRP-LCx* in ECs was completely Relish-dependent (**Fig 5D**), arguing against a role of the TAK1-JNK branch in this process. Although it is unclear at this stage how JNK signaling is activated by enteric infection, Imd and JNK signaling encompass two independent infection-induced pathways whose cooperation is required for EC shedding.

Relish-dependent inhibition of *GATAe* is Required for EC Shedding

Next, we explored the molecular processes downstream of Imd signaling that promote EC shedding. An attractive hypothesis is that Relish might regulate a factor

that promotes cell detachment. The GATA transcription factor GATAe has been implicated in the maintenance of midgut compartmentalization (Buchon et al., 2013b). Depleting *GATAe* in ECs led to massive EC death via apical extrusion (**Fig 7A**). *GATAe*-deficient ECs also showed dramatic induction of *CB-mCherry* and *upd3.1-lacZ* reporters (**Fig 7A and S7C**). The crucial role of GATAe in EC survival prompted us to examine whether *GATAe* is repressed by the Imd pathway upon infection, a process that would permit ECs to delaminate. To test this hypothesis, we first analyzed the kinetics of *GATAe* transcription in the midgut following *Ecc15* infection by qPCR (**Fig 7B**). A 40% reduction of *GATAe* was observed at 4 hours post infection, a time point when the mitotic response is just about to begin. During the regeneration phase (8 hours post-infection and onwards), the level of *GATAe* transcripts was gradually restored and further reached a slightly higher level than that in unchallenged guts. In contrast to wild-type control, *GATAe* expression was not significantly decreased in *Relish* mutant flies observed at 6 hours post infection although *GATAe* levels in this group showed greater variation (**Fig 7C**). To better visualize the cellular expression of *GATAe* in the midgut, we examined, using reporter genes, over 6kb regulatory sequences upstream of *GATAe* (**Fig S6A-E**). Expression of the *GATAe* reporter was indeed decreased in ECs at 4 hours post infection with *Ecc15*, notably in regions where massive EC shedding usually took place (**Fig 7D and S6C**). In contrast, the high level of *GATAe* expression in midgut progenitors was not affected during infection (**Fig S6C-E**). An increase of progenitor numbers during the regeneration phase could explain the increase of *GATAe* transcription at later time points (**Fig 7B**). Although the repression of *GATAe* by Relish in ECs is likely indirect since no NFκB site was found in the regulatory DNA of *GATAe* responsible for its

expression in ECs, our data show that infection-triggered Imd signaling decreases *GATAe* expression in ECs, a process that promotes EC shedding.

To reinforce the notion that GATAe functions downstream of Imd signaling, we analyzed whether increased expression of *GATAe* could block EC shedding upon Imd activation. Indeed, EC shedding induced upon *Ecc15* infection was suppressed in flies over-expressing *GATAe* (**Fig 7E-F**). Similarly to *Relish* mutant, such flies were also more susceptible to oral infection **(Fig S7A-B)**. Furthermore, *Ecc15* infection and over-expressing *PGRP-LCx*-induced *CB-mCherry* activation was significantly inhibited upon *GATAe* over-expression (**Fig S7C-E**), consistent with a reduction in EC shedding. Conversely, although depleting *GATAe* in ECs was associated with low-level activation of Imd signaling under basal conditions as indicated by the levels of *pirk*, *PGRP-LB* and *Dpt* expression (**Fig S7C**), inhibiting the Imd pathway did not suppress EC shedding induced by the loss of *GATAe* (**Fig S7F**). This is consistent with a role of *GATAe* downstream of Imd signaling. It is likely that the primary cause for EC shedding upon *GATAe* depletion was excessive JNK activation rather than Imd activity **(Fig S7G)**, but this requires further investigation. Collectively, our data are consistent with a model in which Imd promotes EC shedding upon infection by decreasing *GATAe* expression, which in turn further amplifies JNK activity over a threshold required for EC shedding.

DISCUSSION

Intestinal infection in *Drosophila* triggers the production of ROS and AMPs to combat pathogens and concomitantly drives increased epithelial renewal to repair the collateral damage. Current models propose that epithelial damage is primarily caused

by ROS produced by Duox, while confining the role of the Imd pathway to the induction of antimicrobial peptides (Buchon et al., 2013a). Here we found that the Imd pathway controlled the shedding of intestinal epithelial cells upon infection, challenging the notion that ROS-associated apoptosis is central to EC shedding. Interestingly, the Imd pathway synergized with JNK signaling to induce epithelial cell shedding specifically in the context of bacterial infection and not in other scenarios of EC damage. Furthermore, Imd signaling contributed to cell shedding by decreasing the expression of *GATAe*, a GATA factor critical for EC morphological identity in *Drosophila* (Buchon et al., 2013b). Future studies will be necessary to define the mechanisms by which the Imd pathway regulates *GATAe* and how *GATAe* is linked to epithelial shedding. An intriguing hypothesis is that *GATAe* is required to maintain epithelial cell polarity, whose disruption can lead to JNK activation and cell extrusion (Ohsawa et al., 2018).

In a tissue replenished by the activity of stem cells, such as the intestine, promoting EC shedding likely acts an effective way to dump damaged ECs especially upon infection. This raises the question whether EC shedding *per se* is an integral part of the host intestinal defense. The susceptibility of *Relish* mutant flies to oral infection is usually explained by the defective AMP production (Liehl et al., 2006). Our findings raised an alternative hypothesis, namely that it could be simultaneously due to defects in epithelial turnover. Supporting this notion, over-expression of *GATAe* in ECs inhibited EC shedding and significantly compromised fly survival during infection. Thus, EC shedding may represent an additional layer of the Imd-dependent gut response to pathogenic bacteria, working to enhance host tolerance to infection (Soares et al., 2017) alongside with its well-known function in antibacterial immunity. Indeed, epithelial cell shedding has also been implicated in mammalian mucosal

immunity, where it is associated with the expulsion of infected epithelial cells, thereby reducing the chance of bacterial colonization (Sellin et al., 2015; Sellin et al., 2014).

Using *CB* and AMP reporters, our study uncovered that EC shedding and antibacterial immunity, two Imd-dependent processes, could be simultaneously induced because the two responses were spatially separated. Such cell-specific NFκB responses to infection should well coordinate different host defense strategies, namely resistance and tolerance, for optimal host survival. It is likely that specific transcription factors together with the NFκB factor Relish can shape distinct outputs of Imd activation. In the case of EC shedding, it appears that JNK activity provides the second signal that intersects with Imd activation leading to cell elimination. Consistently, implication of JNK signaling in EC elimination has previously been described in other contexts in the fly gut (Patel et al., 2015; Zhai et al., 2015). Moreover, using both immunity (*Dpt)* and EC shedding (*CB*) reporters, we also showed that ECs were the primary Imd-responsive cell type in the *Drosophila* midgut. Restricting Imd activation to ECs likely serves to protect midgut progenitors from damage.

Our study together with others points to an ancestral link between epithelial immunity and cell shedding. The *Drosophila* Imd pathway mirrors aspects of tumor necrosis factor receptor (TNFR) signaling in mammals (Leulier et al., 2002). Both pathways share many components and signaling steps, notably the ubiquitination and caspase-dependent cleavage of the adaptors Imd and RIP1 respectively, and the involvement of TAK1 kinase and IKK complex for NFκB activation. Of note, epithelium-intrinsic TNFR1 signaling is also necessary and sufficient to trigger intestinal epithelial cell shedding (Marchiando et al., 2011; Piguet et al., 1998;

Vereecke et al., 2011). Thus, the dual functions of the Imd and the TNFR pathways in immunity and epithelial cell shedding extend from flies to mammals. In mammals, additional immune pathways such as Nod-like receptor (NLR) signaling have also been implicated in the shedding of infected intestinal epithelial cells from the mucosa (Knodler et al., 2010; Rauch et al., 2017; Sellin et al., 2014). In contrast, neither fly Toll nor mammalian Toll-like receptor (TLR) signaling has an epithelium-intrinsic role in promoting epithelial shedding (Abreu, 2010; Buchon et al., 2014). However, specific mechanisms that each pathway adopts to regulate shedding may have been diversified during evolution. As shown here, Imd-induced shedding relied entirely on a transcriptional response controlled by the NFκB transcription factor Relish, while NLR-dependent shedding acts via caspase-centered inflammasome activation (Sellin et al., 2015). In contrast, the transcriptional response downstream of NFκB factors partially contributes to the shedding process induced by TNFR1 activation (Williams et al., 2013). Additionally, TNFR1 signaling appears essential for homeostatic enterocyte turnover in mice (Matsuoka and Tsujimoto, 2015), while the role of Imd signaling in shedding was restricted to the context of bacterial infection. Collectively, our findings suggest an evolutionarily conserved genetic program of immunity-induced epithelial cell shedding. In future, comparative studies on the mechanisms of epithelial shedding in diverse organisms should serve to better understand the evolution and diversification of epithelial immunity.

AUTHOR CONTRIBUTIONS

Z.Z. designed the research; Z.Z. and J-P.B. performed experiments; Z.Z. interpreted the data; Z.Z. and B.L. discussed the project and wrote the paper.

ACKNOWLEDGEMENTS

We thank Drs. Claudine Neyen, Zheng Guo and Mark Hanson for comments on the manuscript; Won-Jae Lee, Julien Royet, Sara Cherry, Luis Teixeira, Leanne Jones, Mirka Uhlirova, BDSC, DGRC, VDRC for fly stocks; DSHB for antibodies; the FCCF and BIOP platforms at EPFL for technical help. This project was supported by the SNSF grant 3100A0-12079/1 (to B.L.) and the Hunan Natural Science grant 2018JJ1015 (to Z.Z.). Z.Z. was also supported by a Marie-Curie IEF fellowship (gutENCODE).

DECLARATION OF INTERESTS

The authors declare no competing interests.

REFERENCES

Abreu, M.T. (2010). Toll-like receptor signalling in the intestinal epithelium: how bacterial recognition shapes intestinal function. Nat Rev Immunol *10*, 131-144.

Amcheslavsky, A., Jiang, J., and Ip, Y.T. (2009). Tissue damage-induced intestinal stem cell division in Drosophila. Cell Stem Cell *4*, 49-61.

Barker, N. (2014). Adult intestinal stem cells: critical drivers of epithelial homeostasis and regeneration. Nature reviews Molecular cell biology *15*, 19-33.

Basset, A., Khush, R.S., Braun, A., Gardan, L., Boccard, F., Hoffmann, J.A., and Lemaitre, B. (2000). The phytopathogenic bacteria Erwinia carotovora infects Drosophila and activates an immune response. Proc Natl Acad Sci U S A *97*, 3376-3381.

Biteau, B., Hochmuth, C.E., and Jasper, H. (2008). JNK activity in somatic stem cells causes loss of tissue homeostasis in the aging Drosophila gut. Cell Stem Cell *3*, 442-455.

Blanpain, C., and Fuchs, E. (2014). Stem cell plasticity. Plasticity of epithelial stem cells in tissue regeneration. Science *344*, 1242281.

Bosco-Drayon, V., Poidevin, M., Boneca, I.G., Narbonne-Reveau, K., Royet, J., and Charroux, B. (2012). Peptidoglycan sensing by the receptor PGRP-LE in the

536 Drosophila gut induces immune responses to infectious bacteria and tolerance to
537 microbiota. Cell Host Microbe *12*, 153-165.

538 Broderick, N.A., Buchon, N., and Lemaitre, B. (2014). Microbiota-induced changes in
539 drosophila melanogaster host gene expression and gut morphology. MBio *5*, e01117-
540 01114.

541 Buchon, N., Broderick, N.A., Chakrabarti, S., and Lemaitre, B. (2009a). Invasive and
542 indigenous microbiota impact intestinal stem cell activity through multiple pathways
543 in Drosophila. Genes Dev *23*, 2333-2344.

544 Buchon, N., Broderick, N.A., Kuraishi, T., and Lemaitre, B. (2010). Drosophila
545 EGFR pathway coordinates stem cell proliferation and gut remodeling following
546 infection. BMC Biol *8*, 152.

547 Buchon, N., Broderick, N.A., and Lemaitre, B. (2013a). Gut homeostasis in a
548 microbial world: insights from Drosophila melanogaster. Nat Rev Microbiol *11*, 615-
549 626.

550 Buchon, N., Broderick, N.A., Poidevin, M., Pradervand, S., and Lemaitre, B. (2009b).
551 Drosophila intestinal response to bacterial infection: activation of host defense and
552 stem cell proliferation. Cell Host Microbe *5*, 200-211.

553 Buchon, N., Osman, D., David, F.P., Fang, H.Y., Boquete, J.P., Deplancke, B., and
554 Lemaitre, B. (2013b). Morphological and molecular characterization of adult midgut
555 compartmentalization in Drosophila. Cell Rep *3*, 1725-1738.

556 Buchon, N., Silverman, N., and Cherry, S. (2014). Immunity in Drosophila
557 melanogaster--from microbial recognition to whole-organism physiology. Nat Rev
558 Immunol *14*, 796-810.

559 Coopersmith, C.M., O'Donnell, D., and Gordon, J.I. (1999). Bcl-2 inhibits ischemia-
560 reperfusion-induced apoptosis in the intestinal epithelium of transgenic mice. Am J
561 Physiol *276*, G677-686.

562 Denning, D.P., Hatch, V., and Horvitz, H.R. (2012). Programmed elimination of cells
563 by caspase-independent cell extrusion in C. elegans. Nature *488*, 226-230.

564 DiAngelo, J.R., Bland, M.L., Bambina, S., Cherry, S., and Birnbaum, M.J. (2009).
565 The immune response attenuates growth and nutrient storage in Drosophila by
566 reducing insulin signaling. Proc Natl Acad Sci U S A *106*, 20853-20858.

567 Dutta, D., Xiang, J., and Edgar, B.A. (2013). RNA expression profiling from FACS-
568 isolated cells of the Drosophila intestine. Current protocols in stem cell biology *27*,
569 Unit 2F 2.

570 Erkosar, B., Defaye, A., Bozonnet, N., Puthier, D., Royet, J., and Leulier, F. (2014).
571 Drosophila microbiota modulates host metabolic gene expression via IMD/NF-
572 kappaB signaling. PLoS One *9*, e94729.

573 Georgel, P., Naitza, S., Kappler, C., Ferrandon, D., Zachary, D., Swimmer, C.,
574 Kopczynski, C., Duyk, G., Reichhart, J.M., and Hoffmann, J.A. (2001). Drosophila
575 immune deficiency (IMD) is a death domain protein that activates antibacterial
576 defense and can promote apoptosis. Dev Cell *1*, 503-514.

577 Guo, Z., Lucchetta, E., Rafel, N., and Ohlstein, B. (2016). Maintenance of the adult
578 Drosophila intestine: all roads lead to homeostasis. Curr Opin Genet Dev *40*, 81-86.

579 Jiang, H., and Edgar, B.A. (2012). Intestinal stem cell function in Drosophila and
580 mice. Curr Opin Genet Dev *22*, 354-360.

581 Jiang, H., Grenley, M.O., Bravo, M.J., Blumhagen, R.Z., and Edgar, B.A. (2011).
582 EGFR/Ras/MAPK signaling mediates adult midgut epithelial homeostasis and
583 regeneration in Drosophila. Cell Stem Cell *8*, 84-95.

584 Jiang, H., Patel, P.H., Kohlmaier, A., Grenley, M.O., McEwen, D.G., and Edgar, B.A.
585 (2009). Cytokine/Jak/Stat signaling mediates regeneration and homeostasis in the
586 Drosophila midgut. Cell *137*, 1343-1355.

587 Kleino, A., and Silverman, N. (2014). The Drosophila IMD pathway in the activation
588 of the humoral immune response. Dev Comp Immunol *42*, 25-35.

589 Knodler, L.A., Vallance, B.A., Celli, J., Winfree, S., Hansen, B., Montero, M., and
590 Steele-Mortimer, O. (2010). Dissemination of invasive Salmonella via bacterial-
591 induced extrusion of mucosal epithelia. Proc Natl Acad Sci U S A *107*, 17733-17738.

592 Lee, K.A., Kim, S.H., Kim, E.K., Ha, E.M., You, H., Kim, B., Kim, M.J., Kwon, Y.,
593 Ryu, J.H., and Lee, W.J. (2013). Bacterial-derived uracil as a modulator of mucosal
594 immunity and gut-microbe homeostasis in Drosophila. Cell *153*, 797-811.

595 Lee, K.Z., Lestradet, M., Socha, C., Schirmeier, S., Schmitz, A., Spenle, C., Lefebvre,
596 O., Keime, C., Yamba, W.M., Bou Aoun, R., *et al.* (2016). Enterocyte Purge and
597 Rapid Recovery Is a Resilience Reaction of the Gut Epithelium to Pore-Forming
598 Toxin Attack. Cell Host Microbe *20*, 716-730.

599 Leulier, F., Vidal, S., Saigo, K., Ueda, R., and Lemaitre, B. (2002). Inducible
600 expression of double-stranded RNA reveals a role for dFADD in the regulation of the
601 antibacterial response in Drosophila adults. Curr Biol *12*, 996-1000.

602 Liang, J., Balachandra, S., Ngo, S., and O'Brien, L.E. (2017). Feedback regulation of
603 steady-state epithelial turnover and organ size. Nature *548*, 588-591.

604 Liehl, P., Blight, M., Vodovar, N., Boccard, F., and Lemaitre, B. (2006). Prevalence
605 of local immune response against oral infection in a Drosophila/Pseudomonas
606 infection model. PLoS Pathog *2*, e56.

607 Marchiando, A.M., Shen, L., Graham, W.V., Edelblum, K.L., Duckworth, C.A.,
608 Guan, Y., Montrose, M.H., Turner, J.R., and Watson, A.J. (2011). The epithelial
609 barrier is maintained by in vivo tight junction expansion during pathologic intestinal
610 epithelial shedding. Gastroenterology *140*, 1208-1218 e1201-1202.

611 Marianes, A., and Spradling, A.C. (2013). Physiological and stem cell
612 compartmentalization within the Drosophila midgut. Elife *2*, e00886.

613 Matsuoka, Y., and Tsujimoto, Y. (2015). Role of RIP1 in physiological enterocyte
614 turnover in mouse small intestine via nonapoptotic death. Genes Cells *20*, 11-28.

615 McGuire, S.E., Mao, Z., and Davis, R.L. (2004). Spatiotemporal gene expression
616 targeting with the TARGET and gene-switch systems in Drosophila. Sci STKE *2004*,
617 pl6.

618 Meyer, S.N., Amoyel, M., Bergantinos, C., de la Cova, C., Schertel, C., Basler, K.,
619 and Johnston, L.A. (2014). An ancient defense system eliminates unfit cells from
620 developing tissues during cell competition. Science *346*, 1258236.

621 Micchelli, C.A., and Perrimon, N. (2006). Evidence that stem cells reside in the adult
622 Drosophila midgut epithelium. Nature *439*, 475-479.

623 Mistry, R., Kounatidis, I., and Ligoxygakis, P. (2017). Interaction Between Familial
624 Transmission and a Constitutively Active Immune System Shapes Gut Microbiota in
625 Drosophila melanogaster. Genetics.

626 Neyen, C., Bretscher, A.J., Binggeli, O., and Lemaitre, B. (2014). Methods to study
627 Drosophila immunity. Methods *68*, 116-128.

628 Neyen, C., Poidevin, M., Roussel, A., and Lemaitre, B. (2012). Tissue- and ligand-
629 specific sensing of gram-negative infection in drosophila by PGRP-LC isoforms and
630 PGRP-LE. J Immunol *189*, 1886-1897.

631 Ohsawa, S., Vaughen, J., and Igaki, T. (2018). Cell Extrusion: A Stress-Responsive
632 Force for Good or Evil in Epithelial Homeostasis. Dev Cell *44*, 284-296.

633 Paredes, J.C., Welchman, D.P., Poidevin, M., and Lemaitre, B. (2011). Negative
634 regulation by amidase PGRPs shapes the Drosophila antibacterial response and
635 protects the fly from innocuous infection. Immunity *35*, 770-779.

636 Pastor-Pareja, J.C., Grawe, F., Martin-Blanco, E., and Garcia-Bellido, A. (2004).
637 Invasive cell behavior during Drosophila imaginal disc eversion is mediated by the
638 JNK signaling cascade. Dev Cell *7*, 387-399.

639 Patel, P.H., Dutta, D., and Edgar, B.A. (2015). Niche appropriation by Drosophila
640 intestinal stem cell tumours. Nat Cell Biol *17*, 1182-1192.

641 Patterson, A.M., and Watson, A.J.M. (2017). Deciphering the Complex Signaling
642 Systems That Regulate Intestinal Epithelial Cell Death Processes and Shedding. Front
643 Immunol *8*, 841.

644 Petersen, A.J., Rimkus, S.A., and Wassarman, D.A. (2012). ATM kinase inhibition in
645 glial cells activates the innate immune response and causes neurodegeneration in
646 Drosophila. Proc Natl Acad Sci U S A *109*, E656-664.

647 Pfeiffer, B.D., Jenett, A., Hammonds, A.S., Ngo, T.T., Misra, S., Murphy, C., Scully,
648 A., Carlson, J.W., Wan, K.H., Laverty, T.R., *et al.* (2008). Tools for neuroanatomy
649 and neurogenetics in Drosophila. Proc Natl Acad Sci U S A *105*, 9715-9720.

650 Piguet, P.F., Vesin, C., Guo, J., Donati, Y., and Barazzone, C. (1998). TNF-induced
651 enterocyte apoptosis in mice is mediated by the TNF receptor 1 and does not require
652 p53. Eur J Immunol *28*, 3499-3505.

653 Rauch, I., Deets, K.A., Ji, D.X., von Moltke, J., Tenthorey, J.L., Lee, A.Y., Philip,
654 N.H., Ayres, J.S., Brodsky, I.E., Gronert, K., *et al.* (2017). NAIP-NLRC4
655 Inflammasomes Coordinate Intestinal Epithelial Cell Expulsion with Eicosanoid and
656 IL-18 Release via Activation of Caspase-1 and -8. Immunity *46*, 649-659.

657 Resnik-Docampo, M., Koehler, C.L., Clark, R.I., Schinaman, J.M., Sauer, V., Wong,
658 D.M., Lewis, S., D'Alterio, C., Walker, D.W., and Jones, D.L. (2017). Tricellular
659 junctions regulate intestinal stem cell behaviour to maintain homeostasis. Nat Cell
660 Biol *19*, 52-59.

661 Ryu, J.H., Kim, S.H., Lee, H.Y., Bai, J.Y., Nam, Y.D., Bae, J.W., Lee, D.G., Shin,
662 S.C., Ha, E.M., and Lee, W.J. (2008). Innate immune homeostasis by the homeobox
663 gene caudal and commensal-gut mutualism in Drosophila. Science *319*, 777-782.

664 Schindelin, J., Arganda-Carreras, I., Frise, E., Kaynig, V., Longair, M., Pietzsch, T.,
665 Preibisch, S., Rueden, C., Saalfeld, S., Schmid, B., *et al.* (2012). Fiji: an open-source
666 platform for biological-image analysis. Nat Methods *9*, 676-682.

667 Sellin, M.E., Maslowski, K.M., Maloy, K.J., and Hardt, W.D. (2015). Inflammasomes
668 of the intestinal epithelium. Trends Immunol *36*, 442-450.

669 Sellin, M.E., Muller, A.A., Felmy, B., Dolowschiak, T., Diard, M., Tardivel, A.,
670 Maslowski, K.M., and Hardt, W.D. (2014). Epithelium-intrinsic NAIP/NLRC4
671 inflammasome drives infected enterocyte expulsion to restrict Salmonella replication
672 in the intestinal mucosa. Cell Host Microbe *16*, 237-248.

673 Silverman, N., Zhou, R., Erlich, R.L., Hunter, M., Bernstein, E., Schneider, D., and
674 Maniatis, T. (2003). Immune activation of NF-kappaB and JNK requires Drosophila
675 TAK1. J Biol Chem *278*, 48928-48934.

676 Soares, M.P., Teixeira, L., and Moita, L.F. (2017). Disease tolerance and immunity in
677 host protection against infection. Nat Rev Immunol *17*, 83-96.

678 Tone, S., Sugimoto, K., Tanda, K., Suda, T., Uehira, K., Kanouchi, H., Samejima, K.,
679 Minatogawa, Y., and Earnshaw, W.C. (2007). Three distinct stages of apoptotic
680 nuclear condensation revealed by time-lapse imaging, biochemical and electron
681 microscopy analysis of cell-free apoptosis. Exp Cell Res *313*, 3635-3644.

682 Uhlirova, M., and Bohmann, D. (2006). JNK- and Fos-regulated Mmp1 expression
683 cooperates with Ras to induce invasive tumors in Drosophila. EMBO J *25*, 5294-
684 5304.

685 Vereecke, L., Beyaert, R., and van Loo, G. (2011). Enterocyte death and intestinal
686 barrier maintenance in homeostasis and disease. Trends Mol Med *17*, 584-593.

687 Vidal, S., Khush, R.S., Leulier, F., Tzou, P., Nakamura, M., and Lemaitre, B. (2001).
688 Mutations in the Drosophila dTAK1 gene reveal a conserved function for MAPKKKs
689 in the control of rel/NF-kappaB-dependent innate immune responses. Genes Dev *15*,
690 1900-1912.

691 Williams, J.M., Duckworth, C.A., Watson, A.J., Frey, M.R., Miguel, J.C., Burkitt,
692 M.D., Sutton, R., Hughes, K.R., Hall, L.J., Caamano, J.H., *et al.* (2013). A mouse
693 model of pathological small intestinal epithelial cell apoptosis and shedding induced
694 by systemic administration of lipopolysaccharide. Dis Model Mech *6*, 1388-1399.

695 Zhai, Z., Boquete, J.P., and Lemaitre, B. (2017a). A genetic framework controlling
696 the differentiation of intestinal stem cells during regeneration in Drosophila. PLoS
697 Genet *13*, e1006854.

698 Zhai, Z., Huang, X., and Yin, Y. (2017b). Beyond immunity: The Imd pathway as a
699 coordinator of host defense, organismal physiology and behavior. Dev Comp
700 Immunol.

701 Zhai, Z., Kondo, S., Ha, N., Boquete, J.P., Brunner, M., Ueda, R., and Lemaitre, B.
702 (2015). Accumulation of differentiating intestinal stem cell progenies drives
703 tumorigenesis. Nat Commun *6*, 10219.

704 Zhou, J., Edgar, B.A., and Boutros, M. (2017). ATF3 acts as a rheostat to control JNK
705 signalling during intestinal regeneration. Nat Commun *8*, 14289.

706

707

708 **FIGURE LEGENDS**

Figure 1. Identification of an infection-inducible enhancer fragment of *upd2*

(A) Working model of JAK-STAT signaling in *Drosophila* midgut. Note that shedding enterocytes (ECs) release Upd2 and Upd3 ligands, which bind to the JAK-STAT receptor Domeless (Dome) expressed only in the progenitors (intestinal stem cell (ISC) and enteroblast (EB)).

(B) Cis-regulatory elements of *upd2* tested for enhancer activity. Fragments shown in red are activated in ECs upon *Ecc15* oral infection.

(C-D) Sagittal view (Sag.) of midgut epithelium from unchallenged (UN, C) and infected (*Ecc15*, 10-11 hours post infection (hpi), D) flies. *Myo1A>nlsGFP* labels ECs and *esg-GFP* labels ISCs and EBs, respectively. DAPI stains nuclei. Some shedding cells are indicated with arrows.

(E) Sagittal view of midgut epithelium from *Ecc15*-infected flies carrying both *Myo1A>nlsGFP* (EC marker) and *CB-mCherry* reporter. A shedding EC (orange arrow), a shed EC with ring or necklace-shaped chromatin condensation (white arrow) and two shed ECs showing nuclear collapse and disassembly (yellow arrows) are indicated.

Scale bars 50μm. See also Figure S1.

Figure 2. The *CB* enhancer is regulated by the Imd pathway

(A) Schematic representation of the Imd pathway.

(B-E) *CB-Gal4/UAS-CD8GFP* (*CB>CD8GFP*) expression in the midgut of flies upon different challenges. Bottom panel shows sagittal view highlighting shed cells in the gut lumen.

(F-G) *Dpt, mCherry* (*CB-mCherry*) and *lacZ* (*upd3.1-lacZ*) expression in midguts of unchallenged and *Ecc15*-infected flies (F) or midguts over-expressing *PGRP-LCx* in ECs (G). RNAi was performed for 3 days (F) and 6 days (G), respectively, using $Myo1A^{TS}$ as driver. Means and SEMs (n=3).

(H-J) Immunofluorescence showing the activation of *CB-mCherry* upon over-expression of *Rel-VP16* and *RelD* for 3 days at 29°C.

(K) Expression of various genes upon EC-specific over-expression of *Rel-VP16*, *RelD* or *PGRP-LCx* using $Myo1A^{TS}$ for 4 days. Means and SEMs (n>4).

(L-M) *mCherry* reporter expression in the midgut of *CB-mCherry* and *CB.mtNFκB-mCherry* flies following *Ecc15* infection (10hpi).

(N) qPCR quantification of *mCherry* levels in the midgut of flies with the indicated genotype under basal conditions (UN) and upon infection (*Ecc15*, 10-11hpi). Means and SEMs (n=3).

(O) Differential activation of *CB-mCherry* and *CB.mtNFκB-mCherry* upon EC-specific expression of *Rel-VP16* or *RelD* for 4 days. *pirk* expression was monitored to reveal Imd activity. Means and SEMs (n=3).

***p < 0.001, **p < 0.01, *p < 0.05, ns: p > 0.05; One-way ANOVA. Scale bars 50µm. See also Figure S2.

Figure 3. Different expression pattern of *Dpt* and *CB* reporters along the gut

(A) Schematic representation of the *esgF/O* system.

(B-C) Frontal view of midgut epithelium from flies over-expressing *PGRP-LCx* using *esgF/O* for 4-7 days. White arrows indicate progenitors; yellow arrows indicate newly generated ECs.

(D-F) Expression of *CB* and *Dpt* reporters (*CB-mCherry / Dpt-lacZ*) in the midgut of *Ecc15*-infected flies (D), sagittal view of regions R1 and R4a (E) and quantification of reporter intensity profile of the midgut shown in D (F).

Scale bars 50µm except D 500µm. See also Figure S3.

Figure 4. EC shedding upon infection requires Imd signaling

(A-F) Sagittal view of midgut of *Ecc15*-infected wild-type control (A and C) and Imd pathway deficient flies (10-12hpi). All these flies carry *CB>CD8GFP* reporter. F-Actin is in red.

(G) Quantification of shed cells present in the gut lumen of *Ecc15*-infected control and Imd pathway deficient flies. ***p < 0.001, ns: p > 0.05; One-way ANOVA.

(H-I) Sagittal view of the midgut epithelium from control (H) and *Relish-VP16*-overexpressing flies (I) using $Myo1A^{TS}$ for 4 days.

(J-K) Midgut epithelium from control (J) and flies over-expressing *PGRP-LCx* (K) for 7 days using *esgF/O*. Cells extruding apically into the gut lumen are indicated by arrows.

(L-N) Immunostaining detecting activated Caspase 3 in *Ecc15*-infected flies with indicated genotype (10-12hpi) (L-M) and quantification of Caspase 3 signal intensity (N). ***p < 0.001; Student's *t* test.

Scale bars 50µm.

Figure 5. *Relish* is specifically required for EC shedding upon infection

(A) Midgut mitotic index (PH3 count) of 7 day-old w^{1118} (wild type) and Rel^{E20} isogenic flies infected with *Ecc15* (10hpi).

(B-C) Expression of *upd2*, *upd3* and *Dpt* in wild-type (Rel^{E20}/+) and Rel^{E20} flies under unchallenged conditions (UN) or upon infection (*Ecc15*, 4hpi). B: whole midguts; C: FACS-sorted ECs. Means and SEMs (n=4; ***p < 0.001, **p < 0.01, ns: p > 0.05; One-way ANOVA).

(D) Midgut mitotic index of flies with indicated genotype. $Myo1A^{TS}$ was used as the Gal4 driver. The time window of transgene expression is indicated.

(E) Midgut mitotic index of flies bearing ISC tumors via depletion of *Notch* in progenitor cells, both in wild-type and *Relish* mutant background.

Dots indicate wild-type control; triangles indicate *Relish* mutant background. Means and SEMs in A, D and E (***p < 0.001, **p < 0.01, ns: p > 0.05; Student's *t* test). See also Figure S4.

Figure 6. The JNK pathway cooperates with Imd signaling to induce EC shedding

(A) Kinetics of *puc* expression in midgut of wild-type flies upon *Ecc15* oral infection. Means and SEMs (n=4).

(B) Concurrent detection of JNK activity (puc^{E69}>*GFP*) and *CB-mCherry* expression in flies infected with *Ecc15* (10hpi).

(C) Expression of *Dpt*, *CB-mCherry* and *upd3.1-lacZ* in midgut with EC-specific over-expression of indicated genes for 3-4 days, under both unchallenged conditions (UN) and *Ecc15* infection (11-12hpi). Means and SEMs (n=4).

(D) Representative midgut of indicated flies infected with *Ecc15* (12hpi) showing reduced EC shedding and *CB-mCherry* expression upon JNK inhibition by expressing bsk^{DN} in ECs using $Myo1A^{TS}$.

(E) Quantification of shed cells present in the gut lumen of *Ecc15*-infected wild-type control flies and flies with inhibition of JNK signaling (>bsk^{DN}) or apoptosis (>*p35*) in ECs using $Myo1A^{TS}$.

(F-G) GFP expression (F) in the midgut of *CBM-GFP* and *CBM.mtAP1-GFP* flies following *Ecc15* infection (10hpi), and qPCR quantification of *GFP* expression (G) under basal conditions (UN) and upon infection (10hpi). Means and SEMs (n=3).

(H) *mCherry* expression (from the *CB-mCherry* or *CB.mtNFκB-mCherry* reporter) in midguts over-expressing hep^{CA} in ECs for 15 hours as determined by qPCR. *puc* is used as a readout of JNK activity. Means and SEMs (n=3).
***p < 0.001, ns: p > 0.05; One-way ANOVA. Scale bars 500μm for B, 50μm for D, F and the closeup image in B. See also Figure S5.

Figure 7. Repression of *GATAe* by Relish is required for EC shedding

(A) Sagittal view of the midgut epithelium of wild-type control and flies with EC-specific depletion of *GATAe* for 3 days.

(B) Kinetics of *GATAe* expression in midgut collected after *Ecc15* infection as determined by qPCR. Means and SEMs (n=4; *p < 0.05; One-way ANOVA).

(C) *GATAe* expression level in the midgut of Rel^{E20}/+ (wild type) or Rel^{E20} flies either unchallenged or infected (6hpi). Means and SEMs (*p < 0.05, ns: p > 0.05; One-way ANOVA). Each dot represents one independent measurement.

(D) Expression of the GFP reporter driven by a *GATAe-Gal4* in unchallenged and *Ecc15*-infected midguts. Arrows indicate examples of ECs lacking GFP expression. Prospero (in red) marks EEs.

(E-F) Sagittal view of the midgut epithelium (E) and quantification of shed cells in the gut lumen (F) from *Ecc15*-infected wild-type flies and flies with EC-specific over-expression of *GATAe* for 3 days. Observations were made at 12hpi. Means and SEMs (***p < 0.001; Student's *t* test).

Scale bars 50μm. See also Figures S6-7.

STAR★METHODS

CONTACT FOR REAGENT AND RESOURCE SHARING

Further information and requests for resources and reagents should be directed to and will be fulfilled by the Lead Contact, Bruno Lemaitre (bruno.lemaitre@epfl.ch).

EXPERIMENTAL MODEL AND SUBJECT DETAILS

Drosophila stocks and their use in this study

Driver lines used in the study were *Myo1A-Gal4, tub-Gal80^{TS}, UAS-GFP* (referred as $Myo1A^{TS}$) (Jiang et al., 2009); *esg-Gal4, tub-Gal80^{TS}, UAS-GFP* (referred as esg^{TS}) (Micchelli and Perrimon, 2006); *esg-Gal4, tub-Gal80^{TS}, UAS-GFP*; *UAS-Flp, Act>CD2>Gal4* (referred as *esgF/O*) (Jiang et al., 2009). *UAS-Rel-IR* (KK), *UAS-imd-IR* (KK), *UAS-Dredd-IR* (KK), *UAS-dTAK1-IR* (KK), *UAS-Notch-IR* (KK), *UAS-GATAe-IR* (v10420, GD), *GATAe-Gal4^{VT}* (construct ID: 242357-242360) were obtained

from Vennia *Drosophila* Resource Center (VDRC). The following UAS lines were used, *UAS-PGRP-LCa* (BDSC30917), *UAS-PGRP-LCx* (BDSC30918 and 30919), *UAS-PRGP-LE* (BDSC33054), *UAS-Rel* (BDSC9459), *UAS-Rel-VP16* (BDSC36547), *UAS-RelD* (gift from Sara Cherry), *UAS-Rel68* (BDSC55778), *UAS-Rel49* (BDSC55779), *UAS-Duox-IR* (gift from Won-Jae Lee), *UAS-bsk^{DN}* (BDSC 6409), *UAS-bsk^{DN}* (gift from Mirka Uhlirova, on 3rd chromosome), *UAS-p35* (BDSC5072), *UAS-rpr* (BDSC5824), *UAS-hep^{CA}* (BDSC9306), *UAS-GATAe* (Zhai et al., 2017a), *UAS-GATAe-IR* (BDSC34907), *UAS-mCD8::GFP* (BDSC32185 and 32186). Reporter lines used were *esg::GFP* (gift from Leanne Jones), *upd3.1-lacZ* (Jiang et al., 2011), *Dpt-lacZ* (BDSC30918 and 55707), *Dpt-mCherry* (gift from Julien Royet), *puc^{E69}-lacZ* (DGRC109029), *puc-Gal4^{E69}>UAS-GFP* (Pastor-Pareja et al., 2004), and *upd2* reporters generated in this study. Null mutants for the Imd pathway used were *Rel^{E20}*, *Dredd^{B118}*, *PGRP-LC^{E12}*, *PGRP-LE^{112}*, *TAK1^{D10}* and *imd^{1}*. Isogenic *w^{1118}* and *Rel^{E20}* lines were kindly provided by Luis Teixeira.

w; Myo1A-Gal4, tub-Gal80^{TS}, UAS-GFP; upd2_CB-mCherry, upd3.1-lacZ − used as wild type to visualize shedding ECs (Figures 1C, 1E and S1E) and also used as an EC driver to overexpress UAS-linked transgenes to analyze gene expression or EC shedding (Figures 2F-K, 2O, 4H-I, 6C-E, 6H, 7A and 7E-F; S2A-B, S2E-I, S4A, S5A-B, S7B-E and S7G).

w; esg-Gal4, tub-Gal80^{TS}, UAS-GFP; upd2_CB-mCherry, upd3.1-lacZ − used as an ISC and EB driver to overexpress *UAS-Notch-IR* (Figure S4D).

w; Myo1A-Gal4, tub-Gal80^{TS}, UAS-GFP; and *w; Myo1A-Gal4, tub-Gal80^{TS}, UAS-GFP; Rel^{E20}* – used as an EC driver to overexpress UAS-linked transgenes both in wild-type and *Relish* mutant background (Figures 5D, S4B-C, and S7F).

w; esg-Gal4, tub-Gal80^{TS}, UAS-GFP; and *w; esg-Gal4, tub-Gal80^{TS}, UAS-GFP; Rel^{E20}* – used as an ISC and EB driver to overexpress *UAS-Notch-IR* both in wild-type and *Relish* mutant background (Figures 5E and S4E).

CB-mCherry, Rel^{E20} and *w; Myo1A-Gal4, tub-Gal80^{TS}, UAS-GFP; upd2_CB-mCherry, Rel^{E20}* – used to test *CB-mCherry* expression in *Relish* mutant and to perform a rescue experiment (Figures 2N and S2K).

w; Myo1A-Gal4, tub-Gal80^{TS}, UAS-GFP; upd2_CB.mtNFκB-mCherry – used to test *mCherry* expression controlled by *upd2_CB* enhancer with a mutated NFκB motif (Figures 2O, 6H, and S5B).

w; ; upd2_CB-mCherry and *w; upd2_CB-Gal4, UAS-mCD8::GFP;* – used to visualize EC shedding upon different treatments (Figures 2B-E, 2L-N, S1F-G and S2C-D) and in various genetic backgrounds (Figures 2H-J, 3B, 4A-G, 4J-K, 6D-E, 7A and 7E-F; S2E-H, S2J-K, S3A-C, S4D, S5A and S7D).

w; esg-Gal4, tub-Gal80^{TS}, UAS-GFP; UAS-Flp, Act>CD2>Gal4 (*esgF/O*) – used to performed clonal analyses (Figures 3B-C, 4J-K, S3A-D and S5F).

***Drosophila* husbandry**

Female flies were used in all experiments. Fly strains were kept on a standard medium (maize flour, dead yeast, agar and fruit juice) at room temperature, unless otherwise indicated. The age and rearing of flies used were noted within the text, figures, legends, and STAR Methods. In most cases, the driver lines (*Myo1A^{TS}*, *esg^{TS}* or *esgF/O*) were crossed to the *w^{1118}* strain, and the progenies were used as control for over-expression experiments.

METHOD DETAILS

Generation of transgenic reporter lines

pBPGUw-eGFP/mCherry gateway reporter vectors were constructed by replacing the *Gal4* coding sequences and yeast terminator in the *pPBGUw* vector (Pfeiffer et al., 2008) with *eGFP* or *mCherry* coding sequences as KpnI-HindIII fragments (Zongzhao Zhai and Ingrid Lohmann, unpublished). To generate reporter constructs, primers shown below were used to amplify the regulatory regions of *upd2*. The PCR products were first cloned into *pENTR-D-TOPO* (ThermoFisher Scientific) vector, and then swapped into *pBPGUw*, *pBPGUw-eGFP* or *pBPGUw-mCherry* destination vector. Site-specific integration was performed to insert the transgenic reporters at predefined genomic locations. The transgene insertion sites were indicated in Figure S1A. Putative transcription factor binding sites were mutated via overlapping PCR whereby point mutations were introduced through PCR primers. The following motifs, NFκB (GTGAATTCCC→GTTCGTGTTC) and AP1 (TGAATCA→CCAATGG),

were mutated in the way indicated above. Transgenic reporters controlled by the mutated *CB* or *CBM* fragment were inserted in the *attP2* site, and reporter expression level was compared to the wild-type *CB* or *CBM* reporter at the same *attP2* site. All the constructs were verified by sequencing.

Oral infection of adult flies

Bacterial strains *Erwinia carotovora carotovora15* (*Ecc15*), *Ecc15 ΔPyrE* (gift from Won-Jae Lee), *Micrococcus luteus*, *Pseudomonas entomophila gacA*, *Serratia marcescens* Db11 were grown in LB medium at 29°C with shaking overnight, and harvested by centrifugation at 3000g at 4°C for 30 minutes. The pellet was then re-suspended in the residual LB. 4-7 day-old mated female flies (15-20 per vial) were first dry-starved in an empty tube for 2 hours, and then transferred into a classical fly food vial containing a filter paper that totally covers the food and was soaked with a solution consisting of 140µL 2.5% sucrose and bacteria at final OD_{600}100-200, except for *Serratia marcescens* Db11 at final OD_{600}50. Unchallenged control flies were fed with 140µL 2.5% sucrose. Infected flies were kept at 29°C until dissection.

Conditional expression of UAS-linked transgenes

The TARGET system was used in combination with the indicated Gal4 drivers to conditionally express UAS-linked transgenes (McGuire et al., 2004). Flies were grown at 18-22°C to limit Gal4 activity. After being maintained 3-4 days at 18-22°C, newly hatched adult flies with the appropriate genotypes were shifted to 29°C, a temperature inactivating the temperature-sensitive Gal80's ability to suppress Gal4 and in turn allowing for the expression of UAS-linked transgenes in cell-type and/or tissue-specific manner, and dissected after indicated time of transgene activation.

Mosaic analysis was done using the *esgF/O* system (*esg-Gal4, tub-Gal80^{TS}, UAS-GFP*; *UAS-Flp, Act>CD2>Gal4*) (Jiang et al., 2009). Combining the TARGET system, this tool allows activating *UAS-Flp* recombinase in progenitor cells with *esg^{TS}* by temperature shift. Flp in turn excises the CD2 cassette from *Act>CD2>Gal4* (> indicates the FRT site recognized by the Flp) and converts it to a ubiquitous *Act-Gal4* driver that is inherited in the stem cell progenies. ECs were identified by their large nuclei size, round cell shape and relatively weak GFP signal compared to progenitor cells. UAS-linked transgenes were only expressed in cells indicated by the presence of GFP.

Immunohistochemistry

Flies were transferred overnight into a classical fly food vial containing a filter paper soaked with a solution consisting of 5% sucrose to clean the digestive tract. Then, intestines of adult females were dissected in phosphate-buffered saline (PBS), and fixed for at least one hour at room temperature in 4% paraformaldehyde (PFA) in PBS. Flies infected with bacteria were directly dissected for staining. They were subsequently rinsed in PBS+0.1% Triton X-100 (PBT), permeabilized and blocked in 2% BSA 1% NGS PBT for one hour, and incubated with primary antibodies in 2% BSA 1% NGS PBT overnight at 4°C. After one hour of washing, secondary antibodies, DAPI and phalloidin when necessary were applied at room temperature for two hours.

Primary antibodies used are: mouse anti-Pros (1:100), rabbit anti-pH3 (1:1000), rabbit anti-Cleaved Casp3 (1:100), Chicken anti-GFP (1:1000), mouse anti-βGal (1:1000), and Rat anti-mCherry (1:500). Alexa488-, Alexa555- or Alexa647-conjugated secondary antibodies (ThermoFisher Scientific) were used at a final concentration of 1:1000. Nuclei were counterstained by DAPI (1:10'000). Filamentous actin (F-actin) was visualized by phalloidin (1:100) staining.

Image acquisition and processing

All the images were taken on a Zeiss LSM 700 confocal microscope by using a 20x objective. Images were processed using Fiji-Image J and Adobe Photoshop software. Shown in figures are maximal intensity projections of all the confocal *z* stacks. Sagittal view (indicated by "Sag." in Figures) was shown to highlight the dying cells present in the gut lumen, and other pictures were frontal view.

Enterocyte sorting through FACS

w; Myo1A^{TS}; Rel^{E20} virgin females were crossed to either isogenic *w^{1118}* or isogenic *Rel^{E20}* at 25°C. Eclosed progenies (control: *w; Myo1A^{TS}/+; Rel^{E20}/+*; *Relish* mutant: *w; Myo1A^{TS}/+; Rel^{E20}/Rel^{E20}*) were maintained at 25°C for 4-6 days, and then shifted to 29°C for at least 24hours to activate *Myo1A>GFP* that labels ECs prior to an *Ecc15* infection. Oral infection with *Ecc15* was performed as described above. Around 30 flies for each biological replicate were dissected in ice-cold 1xPBS made with DEPC-treated water. Four biological replicates were performed. Cell dissociation and FACS sorting were performed as described (Dutta et al., 2013). ECs were directly sorted into lysis buffer, and total

RNA was isolated using RNeasy mini kit (Qiagen). Around 10ng total RNA was used for cDNA synthesis and subsequent qPCR.

qRT-PCR analysis of gene expression

Total RNA was extracted from dissected midguts (15-20 guts per sample) using Trizol. cDNA was synthesized using the PrimeScript RT reagent Kit (TaKaRa). 0.5µg total RNA was used for reverse transcription with oligo dT, and the 1st strand cDNA was diluted 10-20 times with water and further used in real time PCR. Real time PCR was performed in at lease duplicate for each sample using SYBR Green (Roche) on a LightCycler 480 System (Roche). Expression values were calculated using the ΔΔCt method and relative expression was normalized to *Rp49*. The expression in control sample was further normalized to 1. Primer sequences used for qPCR are available upon request**.**

Lifespan analysis

Genetic crosses were set up at 18-20°C to avoid developmental effects using the TARGET system, and progenies were collected and mated for 3-4 days at 18-20°C. Then, female flies (20-30 per vial) were shifted to 29°C to induce transgene expression. Isogenic w^{1118} and Rel^{E20} flies were grown at 25°C. Flies were infected in triplicates with *Ecc15* at OD_{600}100-200 as described above and kept at 29°C. New *Ecc15* were added every two days, and dead flies were counted daily.

QUANTIFICATION AND STATISTICAL ANALYSIS

For all quantifications, *n* represents the number of biological replicate, and error bar represents SEM. Each independent test was performed typically with 12-15 midguts, unless otherwise noted. Statistical significance was determined using either the unpaired *t* test or one-way ANOVA with Tukey *post hoc* tests where multiple comparisons were necessary, in GraphPad Prism Software, and expressed as *P* values. (*) denotes $p < 0.05$, (**) denotes $p < 0.01$, (***) denotes $p < 0.001$, and (ns) denotes values whose difference was not significant.

Results of mRNA expression obtained with qPCR are shown as mean ± SEM of at least 3 independent biological samples (Figures 2F-G, 2K, 2N-O, 5B-C, 6A, 6C, 6G-H and 7B-C; S2A, S2I, S4A, S4C, S5C-E, S7C, S7E and S7G). Quantification of Casp3 signal intensity in regions of interest (ROI) (Figure 4N) and analysis of line profiles of relative expression level of *Dpt* and *CB* reporters (Figures 3F and S3F) were directly done with Fiji software. Midgut mitotic index was calculated by manually counting PH3-positive progenitor cells along the length of the midgut, and the results (Figures 5A and 5E) are representative of three independent analyses. Fiji macros for automated counting of nuclei in ROI (Figures 4G, 6E and 7F; S2B) or for simultaneously measuring the intensity of *CB* reporter expression and the distance of respective cell nuclei to the tissue border in sagittal confocal sections (Figure S1F), were kindly developed by Dr. Romain Guiet at the BioImaging & Optics Platform (BIOP) in EPFL. The image window of ROI was set to 320 µm x 320 µm when preforming confocal scanning. The macros are available upon request. Survival data were pooled and analyzed in Prism software using the log-rank test (Figures S7A-B). In Figures 4G, 4N, 5A, 5D-E, 6E, 7F and S2B, one dot or one triangle represents one gut.

KEY RESOURCES TABLE

REAGENT or RESOURCE	SOURCE	IDENTIFIER
Antibodies		
Chicken polyclonal anti-GFP	Abcam	Cat# ab13970; RRID: AB_300798
Mouse monoclonal anti-βGal	Sigma-Aldrich	Cat# G8021; RRID: AB_259970
Rat monoclonal anti-mCherry	ThermoFisher Scientific	Cat# M11217; RRID: AB_2536611
Rabbit polyclonal anti-phospho-Histone H3 (Ser10)	Millipore	Cat# 06-570; RRID: AB_310177
Mouse monoclonal anti-Prospero	DSHB	Cat# MR1A; RRID: AB_528440
Rabbit monoclonal anti-Cleaved Caspase-3	Cell Signaling	Cat# 9664; RRID: AB_2070042
Goat anti-Chicken IgY (H+L) Secondary Antibody, Alexa Fluor 488	ThermoFisher Scientific	Cat# A11039; RRID: AB_2534096
Goat anti-Rat IgG (H+L) Cross-Adsorbed Secondary Antibody, Alexa Fluor 555	ThermoFisher Scientific	Cat# A21434; RRID: AB_2535855
Goat anti-Mouse IgG (H+L) Highly Cross-Adsorbed Secondary Antibody, Alexa Fluor 555	ThermoFisher Scientific	Cat# A21424; RRID: AB_141780
Goat anti-Rabbit IgG (H+L) Cross-Adsorbed Secondary Antibody, Alexa Fluor 555	ThermoFisher Scientific	Cat# A21428; RRID: AB_2535849
Goat anti-Mouse IgG (H+L) Highly Cross-Adsorbed Secondary Antibody, Alexa Fluor 647	ThermoFisher Scientific	Cat# A21236; RRID: AB_2535805
Bacterial and Virus Strains		
Erwinia carotovora carotovora15	(Basset et al., 2000)	N/A
Erwinia carotovora carotovora15 ΔPyrE	Won-Jae Lee; (Lee et al., 2013)	N/A
Micrococcus luteus	(Neyen et al., 2014)	N/A
Pseudomonas entomophila gacA	(Liehl et al., 2006)	N/A
Serratia marcescens Db11	(Lee et al., 2016)	N/A
Biological Samples		
Chemicals, Peptides, and Recombinant Proteins		
4',6-Diamidino-2-phenylindole dihydrochloride (DAPI)	Sigma-Aldrich	Cat# D9542; CAS: 28718-90-3
Alexa Fluor 488 Phalloidin	ThermoFisher Scientific	Cat# A12379
Alexa Fluor 555 Phalloidin	ThermoFisher Scientific	Cat# A34055
Dextran sulfate sodium salt from *Leuconostoc* spp, low sulfate content, Mr ~40,000	Sigma-Aldrich	Cat# 53423; CAS: 9011-18-1
Paraformaldehyde 16% solution, EM grade	Electron Microscopy Sciences	Cat# 15710
Critical Commercial Assays		
PrimeScript RT reagent Kit	TaKaRa	RR037A
FastStart Universal SYBR Green Master (ROX)	Roche	04913850001

Deposited Data		
Experimental Models: Cell Lines		
Experimental Models: Organisms/Strains		
D. melanogaster: *w; Myo1A-Gal4, tub-Gal80^{TS}, UAS-GFP;*	Huaqi Jiang; (Jiang et al., 2009)	N/A
D. melanogaster: *w; esg-Gal4, tub-Gal80^{TS}, UAS-GFP;*	Craig Micchelli; (Micchelli and Perrimon, 2006)	N/A
D. melanogaster: *w; esg-Gal4, tub-Gal80^{TS}, UAS-GFP; UAS-Flp, Act>CD2>Gal4*	Bruce Edgar; (Jiang et al., 2009)	N/A
D. melanogaster: *w; UAS-Rel-IR(KK);*	Vienna *Drosophila* Resource Center	VDRC: 108469; FlyBase: FBst0480279
D. melanogaster: *w; UAS-imd-IR(KK);*	Vienna *Drosophila* Resource Center	VDRC: 101834; FlyBase: FBst0473707
D. melanogaster: *w; UAS-Dredd-IR(KK);*	Vienna *Drosophila* Resource Center	VDRC: 104726; FlyBase: FBst0476565
D. melanogaster: *w; UAS-dTAK1-IR(KK);*	Vienna *Drosophila* Resource Center	VDRC: 101357; FlyBase: FBst0473230
D. melanogaster: *w; UAS-Notch-IR(KK);*	Vienna *Drosophila* Resource Center	VDRC: 100002; FlyBase: FBst0471876
D. melanogaster: *y[1] w[*]; ; P{w[+mC]=UAS-PGRP-LC.a}3*	Bloomington *Drosophila* Stock Center	BDSC: 30917; FlyBase: FBst0030917
D. melanogaster: *w[*]; P{w[+mC]=UAS-PGRP-LC.x}2; P{ry[+t7.2]=Dipt2.2-lacZ}3, PGRP-LC[1] ca[1]/TM6B, Tb[1]*	Bloomington *Drosophila* Stock Center	BDSC: 30918; FlyBase: FBst0030918
D. melanogaster: *y[1] w[*]; ; P{w[+mC]=UAS-PGRP-LC.x}1*	Bloomington *Drosophila* Stock Center	BDSC: 30919; FlyBase: FBst0030919
D. melanogaster: *w[*]; P{w[+mC]=UAS-PGRP-LE.FLAG}2;*	Bloomington *Drosophila* Stock Center	BDSC: 33054; FlyBase: FBst0033054
D. melanogaster: *w[1118]; P{w[+mC]=UAS-Rel.His6}2; l(3)*[*]/TM3, Sb[1]*	Bloomington *Drosophila* Stock Center	BDSC: 9459; FlyBase: FBst009459
D. melanogaster: *P{w[+mC]=UAS-Rel.HA-VP16}9F, w[*]; ;*	Bloomington *Drosophila* Stock Center	BDSC: 36547; FlyBase: FBst0036547
D. melanogaster: *w; UAS-RelD;*	Sara Cherry; (DiAngelo et al., 2009)	FlyBase: FBtp0092383
D. melanogaster: *w[*]; P{w[+mC]=UAS-FLAG-Rel.68}i21-B; TM2/TM6C, Sb[1]*	Bloomington *Drosophila* Stock Center	BDSC: 55778; FlyBase: FBst0055778
D. melanogaster: *w[*]; P{w[+mC]=UAS-Rel-V5.49}2;*	Bloomington *Drosophila* Stock Center	BDSC: 55779; FlyBase: FBst0055779
D. melanogaster: *UAS-Duox-IR #1*	Won-Jae Lee; (Lee et al., 2013)	FlyBase: FBtp0021471
D. melanogaster: *UAS-Duox-IR #2*	Won-Jae Lee; (Lee et al., 2013)	FlyBase: FBtp0021471
D. melanogaster: *w[1118] P{w[+mC]=UAS-bsk.DN}2; ;*	Bloomington *Drosophila* Stock Center	BDSC: 6409; FlyBase: FBst006409
D. melanogaster: *w; ; UAS-bsk^{DN}*	Mirka Uhlirova; (Uhlirova and Bohmann, 2006)	N/A
D. melanogaster: *w[*]; P{w[+mC]=UAS-p35.H}BH1;*	Bloomington *Drosophila* Stock Center	BDSC: 5072; FlyBase: FBst005072

D. melanogaster: *w[1118]; P{w[+mC]=UAS-rpr.C}14;*	Bloomington *Drosophila* Stock Center	BDSC: 5824; FlyBase: FBst005824
D. melanogaster: *w[*]; P{w[+mC]=UAS-Hep.Act}2;*	Bloomington *Drosophila* Stock Center	BDSC: 9306; FlyBase: FBst009306
D. melanogaster: *w[*]; ; P{y[+t7.7] w[+mC]=10XUAS-IVS-mCD8::GFP}attP2*	Bloomington *Drosophila* Stock Center	BDSC: 32185; FlyBase: FBst0032185
D. melanogaster: *w[*]; P{y[+t7.7] w[+mC]=10XUAS-IVS-mCD8::GFP}attP40;*	Bloomington *Drosophila* Stock Center	BDSC: 32186; FlyBase: FBst0032186
D. melanogaster: *; esg-GFP[P01986];*	Leanne Jones; (Resnik-Docampo et al., 2017)	FlyBase: FBtp0051138
D. melanogaster: *w; ; upd3.1-lacZ*	Bruce Edgar; (Jiang et al., 2011)	FlyBase: FBtp0085248
D. melanogaster: *P{ry[+t7.2]=Dipt2.2-lacZ}1, P{w[+mC]=Drs-GFP.JM804}1, y[1] w[*]; ;*	Bloomington *Drosophila* Stock Center	BDSC: 55707; FlyBase: FBst0055707
D. melanogaster: *yw; ; Dpt-mCherry.C1*	Bloomington *Drosophila* Stock Center	BDSC: 55706; FlyBase: FBst0055706
D. melanogaster: *w; upd2_C-Gal4.attP16;*	This paper	N/A
D. melanogaster: *w; upd2_CB-Gal4.attP16;*	This paper	N/A
D. melanogaster: *w; ; upd2_CB-mCherry.attP2*	This paper	N/A
D. melanogaster: *w; ; upd2_CB.mtNFκB-mCherry.attP2*	This paper	N/A
D. melanogaster: *w; upd2_CB-GFP.attP40;*	This paper	N/A
D. melanogaster: *w; upd2_CBM-GFP.attP16;*	This paper	N/A
D. melanogaster: *w; ; upd2_CBM-GFP.attP2*	This paper	N/A
D. melanogaster: *w; ; upd2_CBM.mtAP1-GFP.attP2*	This paper	N/A
D. melanogaster: *w; ; upd2_CB-mCherry.attP2, Rel[E20]*	This paper	N/A
D. melanogaster: *w; Myo1A-Gal4, tub-Gal80^{TS}, UAS-GFP; upd2_CB-mCherry.attP2, Rel[E20]*	This paper	N/A
D. melanogaster: *w; Myo1A-Gal4, tub-Gal80^{TS}, UAS-GFP; upd2_CB.mtNFκB-mCherry.attP2*	This paper	N/A
D. melanogaster: *w; Myo1A-Gal4, tub-Gal80^{TS}, UAS-GFP; Rel[E20]*	This paper	N/A
D. melanogaster: *w; esg-Gal4, tub-Gal80^{TS}, UAS-GFP; Rel[E20]*	This paper	N/A
D. melanogaster: *w; upd2_CB-Gal4, UAS-mCD8::GFP;*	This paper	N/A
D. melanogaster: *w; Myo1A-Gal4, tub-Gal80^{TS}, UAS-GFP; upd2_CB-mCherry.attp2, upd3.1-lacZ*	This paper	N/A
D. melanogaster: *w; esg-Gal4, tub-Gal80^{TS}, UAS-GFP; upd2_CB-mCherry.attp2, upd3.1-lacZ*	This paper	N/A
D. melanogaster: *w[*]; cno[3] P{A92}puc[E69] / TM6B,abdA-LacZ*	Kyoto Stock Center	Kyoto Stock Center: 109029; FlyBase: FBst0313643
D. melanogaster: *; UAS-GFP; puc-Gal4^{E69}/TM6B*	Enrique Martin-Blanco; (Pastor-Pareja et al., 2004)	FlyBase: FBal0192963
D. melanogaster: *w[1118]; ; ,* isogenic	Luis Teixeira	N/A
D. melanogaster: *w; ; Rel[E20],* isogenic	Luis Teixeira	FlyBase: FBal0101572
D. melanogaster: *yw, Dredd[B118]; ;*	Bloomington *Drosophila* Stock Center	BDSC: 55712; FlyBase: FBst0055712
D. melanogaster: *w; ; PGRP-LC[E12],* isogenic	Luis Teixeira	FlyBase: FBal0212184
D. melanogaster: *yw, PGRP-LE[112]; ;*	Bloomington *Drosophila* Stock Center	BDSC: 33055; FlyBase: FBst0033055
D. melanogaster: *yw, TAK1[D10]; ;*	(Vidal et al., 2001)	FlyBase: FBal0126475

D. melanogaster: *P{ry[+t7.2]=Dipt2.2-lacZ}1; b[*] pr[*] imd[1];*	Bloomington *Drosophila* Stock Center	BDSC: 55711; FlyBase: FBst0055711
D. melanogaster: *w; ; UAS-GATAe 5-1*	(Zhai et al., 2017a)	N/A
D. melanogaster: *w; UAS-GATAe 5-2;*	(Zhai et al., 2017a)	N/A
D. melanogaster: *w; UAS-GATAe-IR(GD);*	Vienna *Drosophila* Resource Center	VDRC: 10420; FlyBase: FBst0450091
D. melanogaster: *y[1] sc[*] v[1]; ; P{y[+t7.7] v[+t1.8]=TRiP.HMS01253}attP2/TM3, Sb[1]*	Bloomington *Drosophila* Stock Center	BDSC: 34907; FlyBase: FBst0034907
D. melanogaster: *; ; GATAe-Gal4[VT042357]*	Vienna *Drosophila* Resource Center	VDRC: 209818
D. melanogaster: *; ; GATAe-Gal4[VT042358]*	Vienna *Drosophila* Resource Center	VDRC: 205732
D. melanogaster: *; ; GATAe-Gal4[VT042359]*	Vienna *Drosophila* Resource Center	VDRC: 214828 (discarded)
D. melanogaster: *; ; GATAe-Gal4[VT042360]*	Vienna *Drosophila* Resource Center	VDRC: 205492 (discarded)
Oligonucleotides		
Primer for cloning of *upd2_1.9kb*, forward: caccACAGTGAGTATGGATCGGTT	Microsynth	https://www.microsynth.ch/dna-oligos.html
Primer for cloning of *upd2_1.9kb*, reverse: GATCACTAGCAGCACCTGCC	Microsynth	https://www.microsynth.ch/dna-oligos.html
Primer for cloning of *upd2_A*, forward: caccCTAGCTGTGCCACGCCCCTC	Microsynth	https://www.microsynth.ch/dna-oligos.html
Primer for cloning of *upd2_A*, reverse: GATTGGTAATTGTGTGTCGC	Microsynth	https://www.microsynth.ch/dna-oligos.html
Primer for cloning of *upd2_B*, forward: caccCATACTTGCCCACGGTAAAG	Microsynth	https://www.microsynth.ch/dna-oligos.html
Primer for cloning of *upd2_B*, reverse: GAGGGGCGTGGCACAGCTAG	Microsynth	https://www.microsynth.ch/dna-oligos.html
Primer for cloning of *upd2_C*, forward: caccTAGCGCCAGGTGCTAAGCTG	Microsynth	https://www.microsynth.ch/dna-oligos.html
Primer for cloning of *upd2_C*, reverse: TGGAAAACTTTACCGTGGGC	Microsynth	https://www.microsynth.ch/dna-oligos.html
Primer for cloning of *upd2_D*, forward: caccTCATAGGCTTTAAAGTGATG	Microsynth	https://www.microsynth.ch/dna-oligos.html
Primer for cloning of *upd2_D*, reverse: GCACATCCAATTAACCCAATC	Microsynth	https://www.microsynth.ch/dna-oligos.html
Primer for cloning of *upd2_CA*, forward: caccTAGCGCCAGGTGCTAAGCTG	Microsynth	https://www.microsynth.ch/dna-oligos.html
Primer for cloning of *upd2_CA*, reverse: AGGATGCCACCATACTATGC	Microsynth	https://www.microsynth.ch/dna-oligos.html
Primer for cloning of *upd2_CB*, forward: caccGCATAGTATGGTGGCATCCT	Microsynth	https://www.microsynth.ch/dna-oligos.html
Primer for cloning of *upd2_CB*, reverse: TGGAAAACTTTACCGTGGGC	Microsynth	https://www.microsynth.ch/dna-oligos.html
Primer for cloning of *upd2_CBM*, forward: caccGTAGCCAGTCCGATTATTCA	Microsynth	https://www.microsynth.ch/dna-oligos.html
Primer for cloning of *upd2_CBM*, reverse: GACATTCGACGGGTGGCACT	Microsynth	https://www.microsynth.ch/dna-oligos.html
Primer for cloning of *upd2_CB-S1*, forward: caccGCATAGTATGGTGGCATCCT	Microsynth	https://www.microsynth.ch/dna-oligos.html
Primer for cloning of *upd2_CB-S1*, reverse: ATATCGCTCCATGGATATAC	Microsynth	https://www.microsynth.ch/dna-oligos.html

Primer for cloning of *upd2_CB-S2*, forward: caccGTATATCCATGGAGCGATAT	Microsynth	https://www.microsynth.ch/dna-oligos.html
Primer for cloning of *upd2_CB-S2*, reverse: CGCGTCGTCAGAGGCTGAAC	Microsynth	https://www.microsynth.ch/dna-oligos.html
Primer for cloning of *upd2_CB-S3*, forward: caccGTTCAGCCTCTGACGACGCG	Microsynth	https://www.microsynth.ch/dna-oligos.html
Primer for cloning of *upd2_CB-S3*, reverse: TGGAAAACTTTACCGTGGGC	Microsynth	https://www.microsynth.ch/dna-oligos.html
Recombinant DNA		
Plasmid: *pBPGUw*	(Pfeiffer et al., 2008)	Addgene Plasmid #17575
Plasmid: *pBPGUw-eGFP*	This paper	N/A
Plasmid: *pBPGUw-mCherry*	This paper	N/A
Plasmid: *pBPGUw_upd2-C*	This paper	N/A
Plasmid: *pBPGUw_upd2-CB*	This paper	N/A
Plasmid: *pBPGUw-mCherry_upd2-CB*	This paper	N/A
Plasmid: *pBPGUw-GFP_upd2-CB*	This paper	N/A
Plasmid: *pBPGUw-mCherry_upd2-CB-mtNFκB*	This paper	N/A
Plasmid: *pBPGUw-GFP_upd2-CBM*	This paper	N/A
Plasmid: *pBPGUw-GFP_upd2-CBM-mtAP1*	This paper	N/A
Software and Algorithms		
Fiji	(Schindelin et al., 2012)	https://www.fiji.sc/
Prism 5	GraphPad	http://www.graphpad.com/scientificsoftware/prism/
Adobe Photoshop CS5	Adobe	http://www.adobe.com
Other		

Figure 1

Click here to download Figure Fig 1-new-lzw.tif

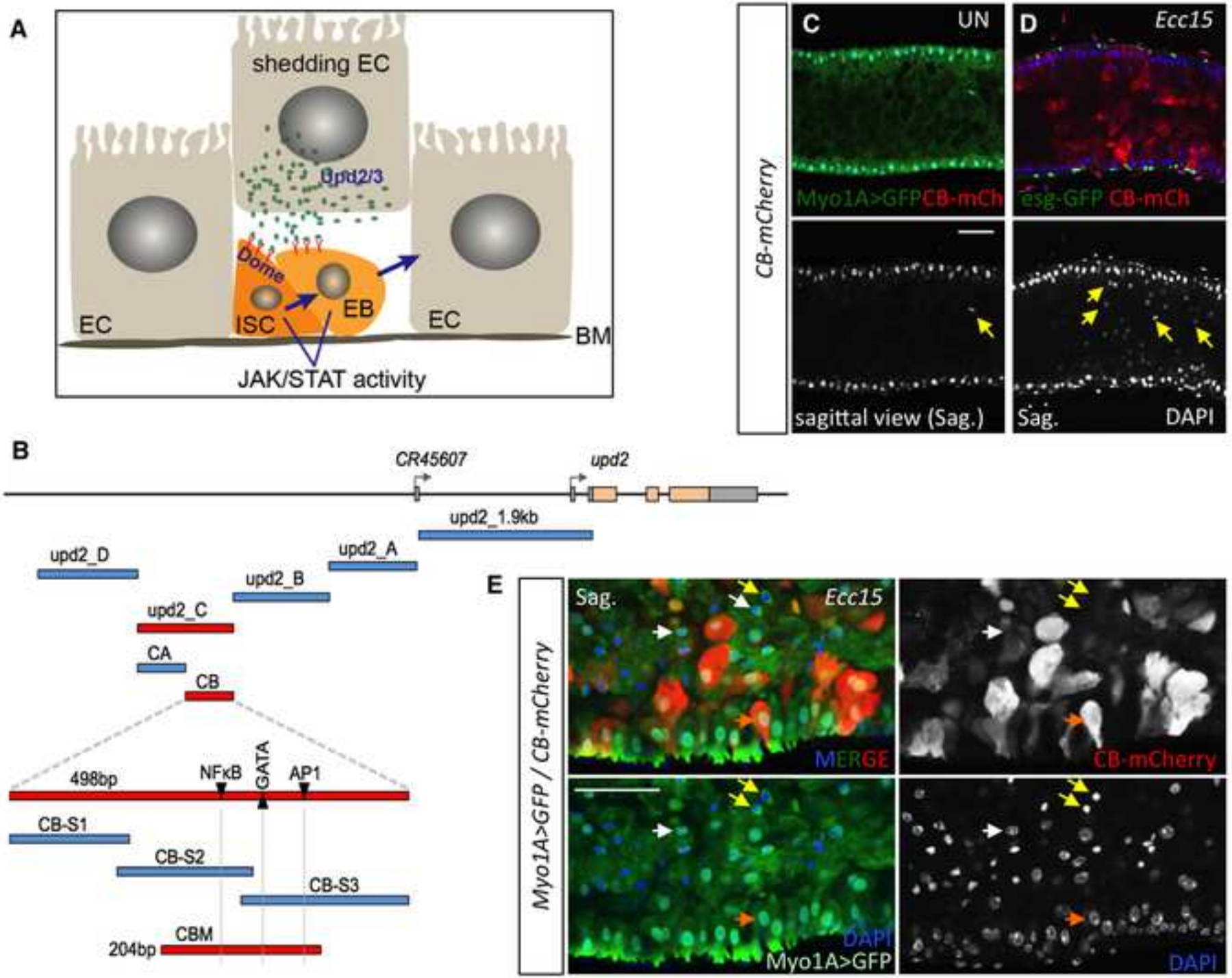

Figure 2

Click here to download Figure Fig 2.tif

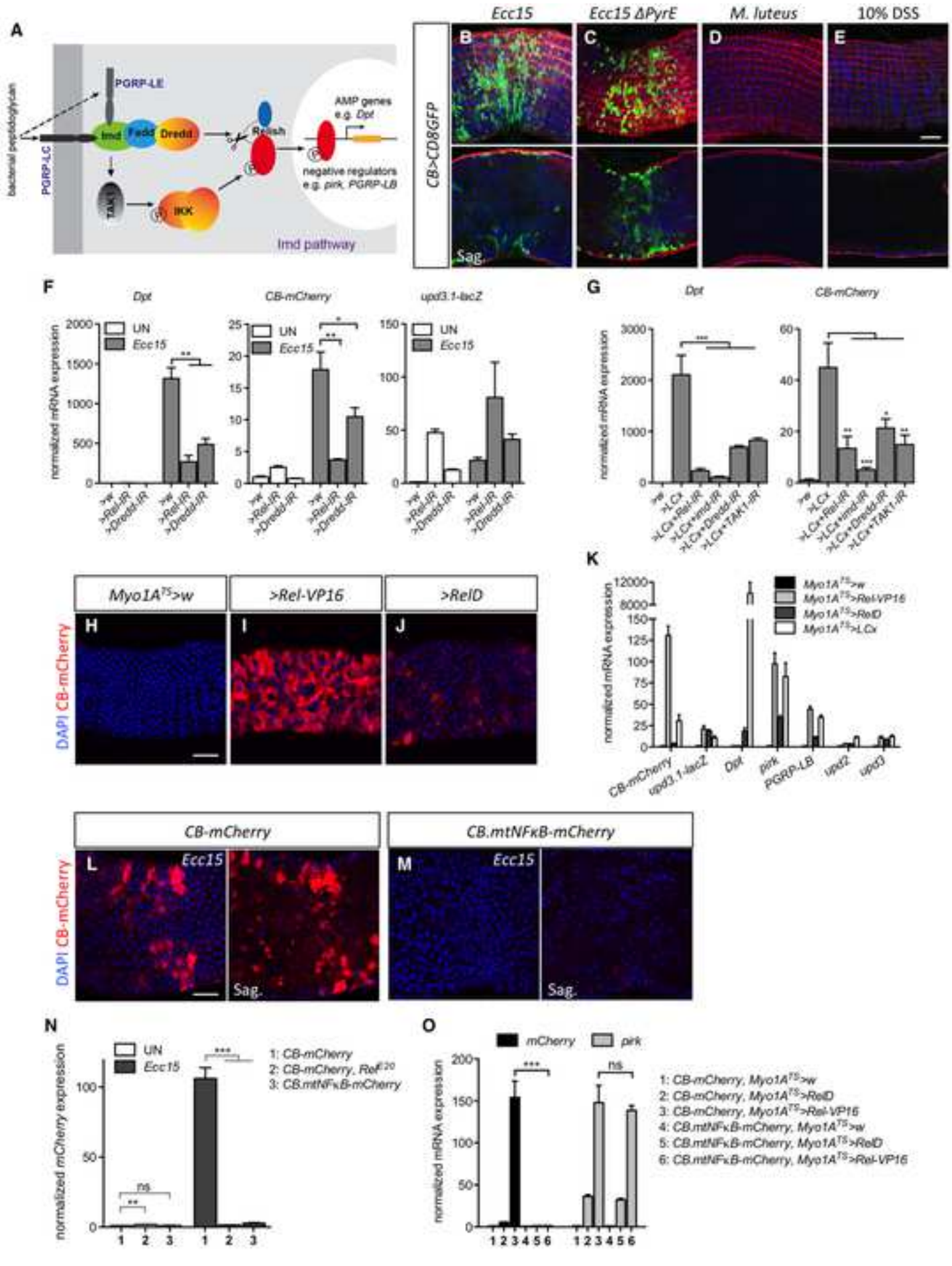

Figure 3

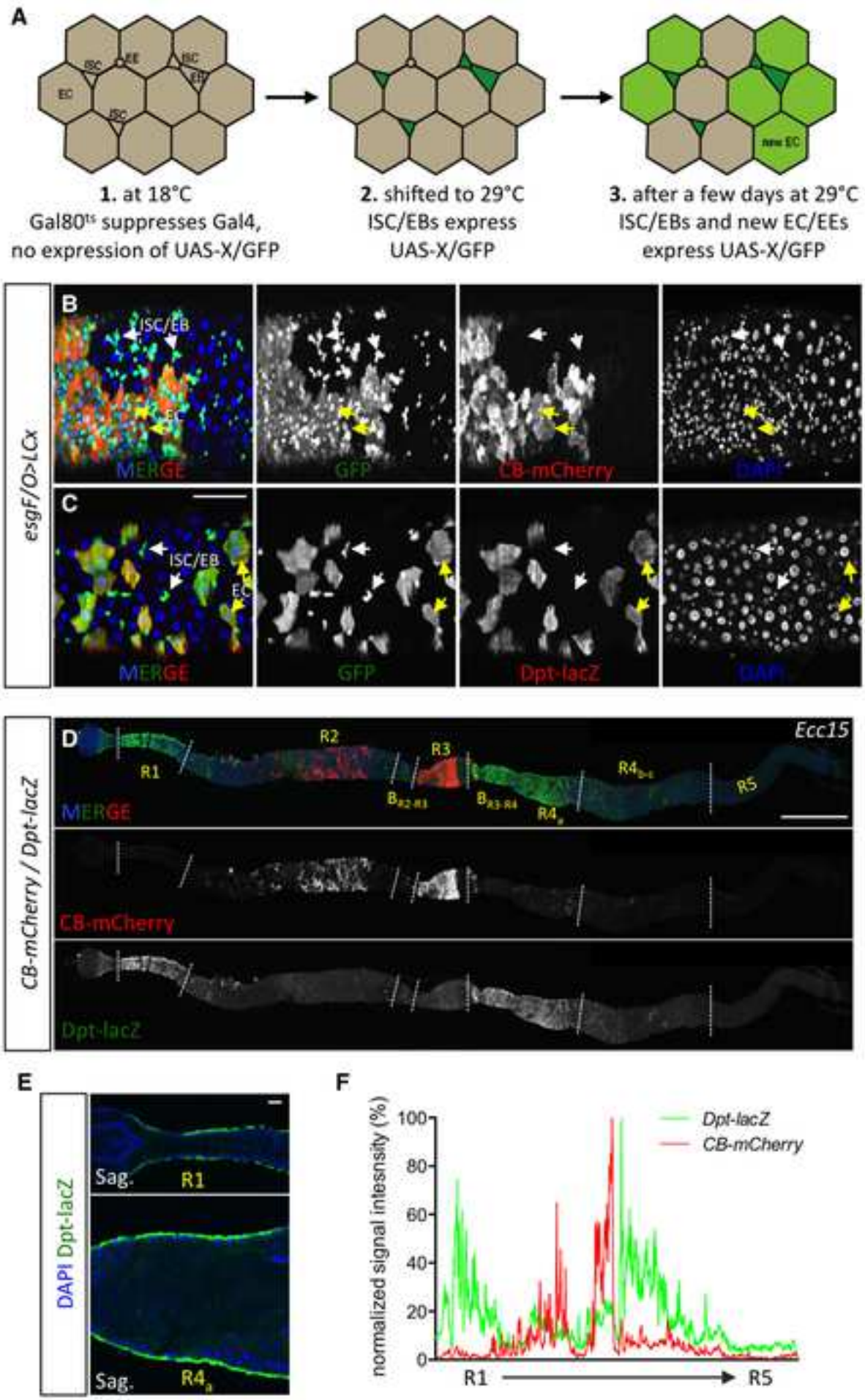

Figure 4

Click here to download Figure Fig 4.tif

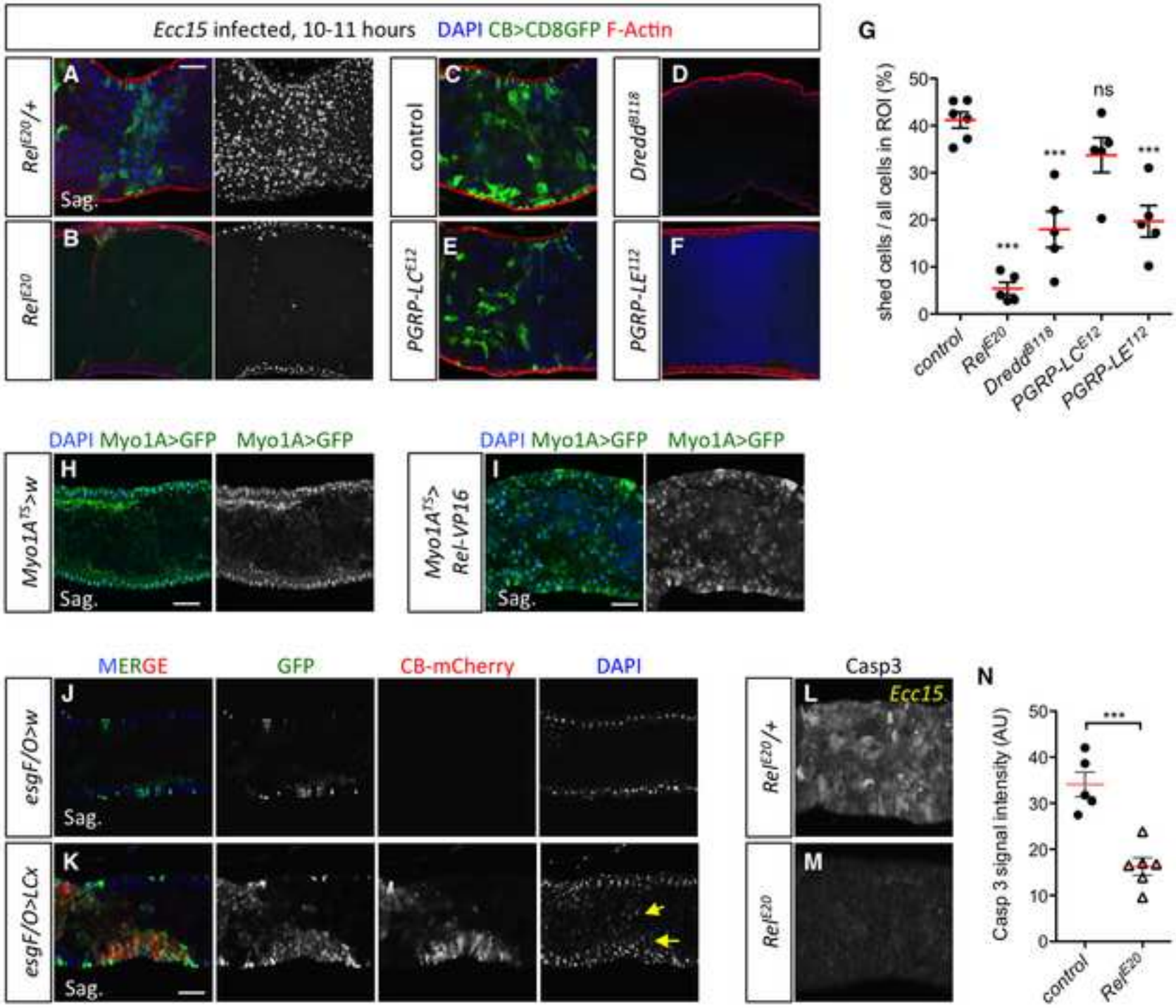

Figure 5

Click here to download Figure Fig 5.tif

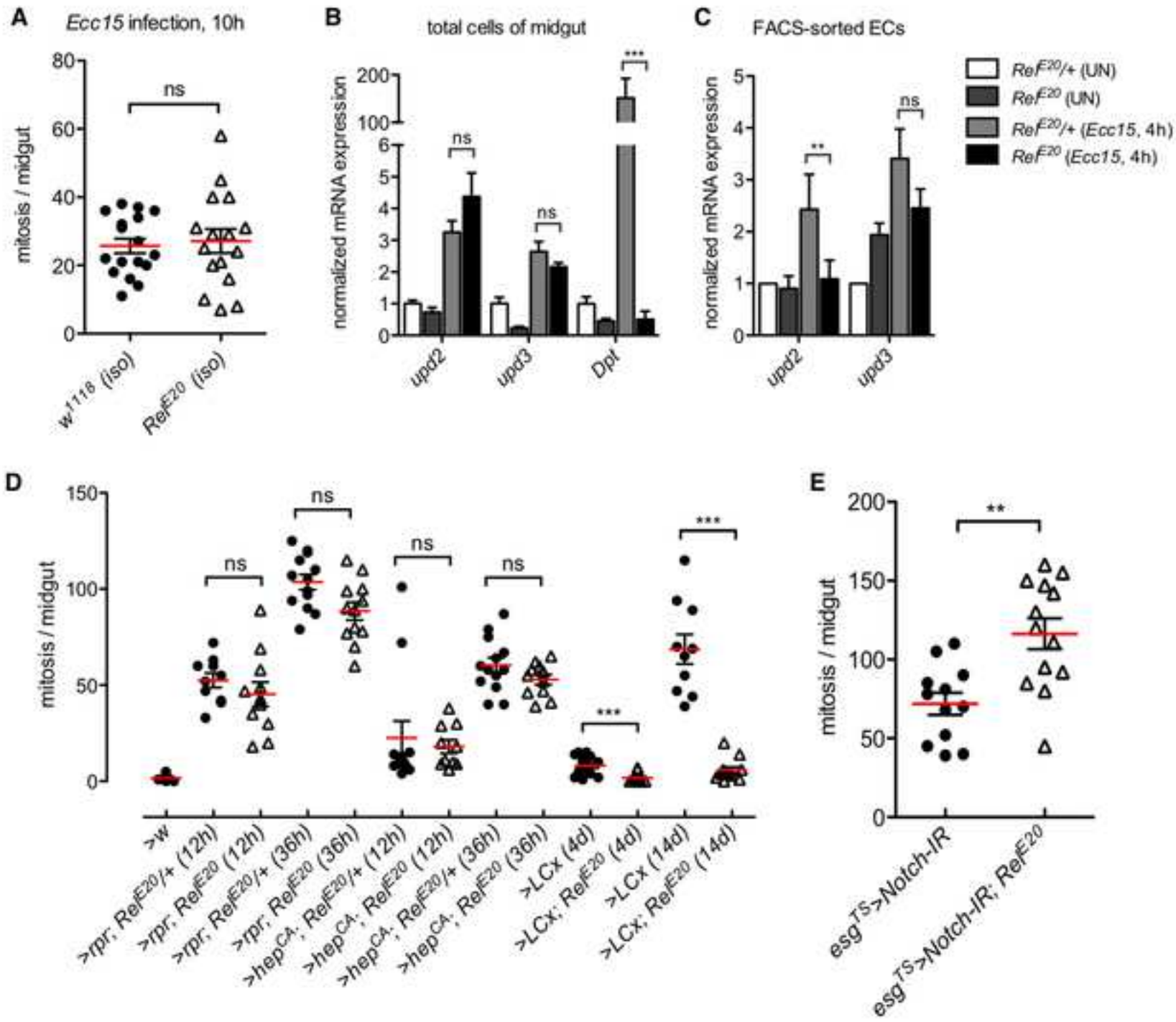

Figure 6

Click here to download Figure Fig 6.tif

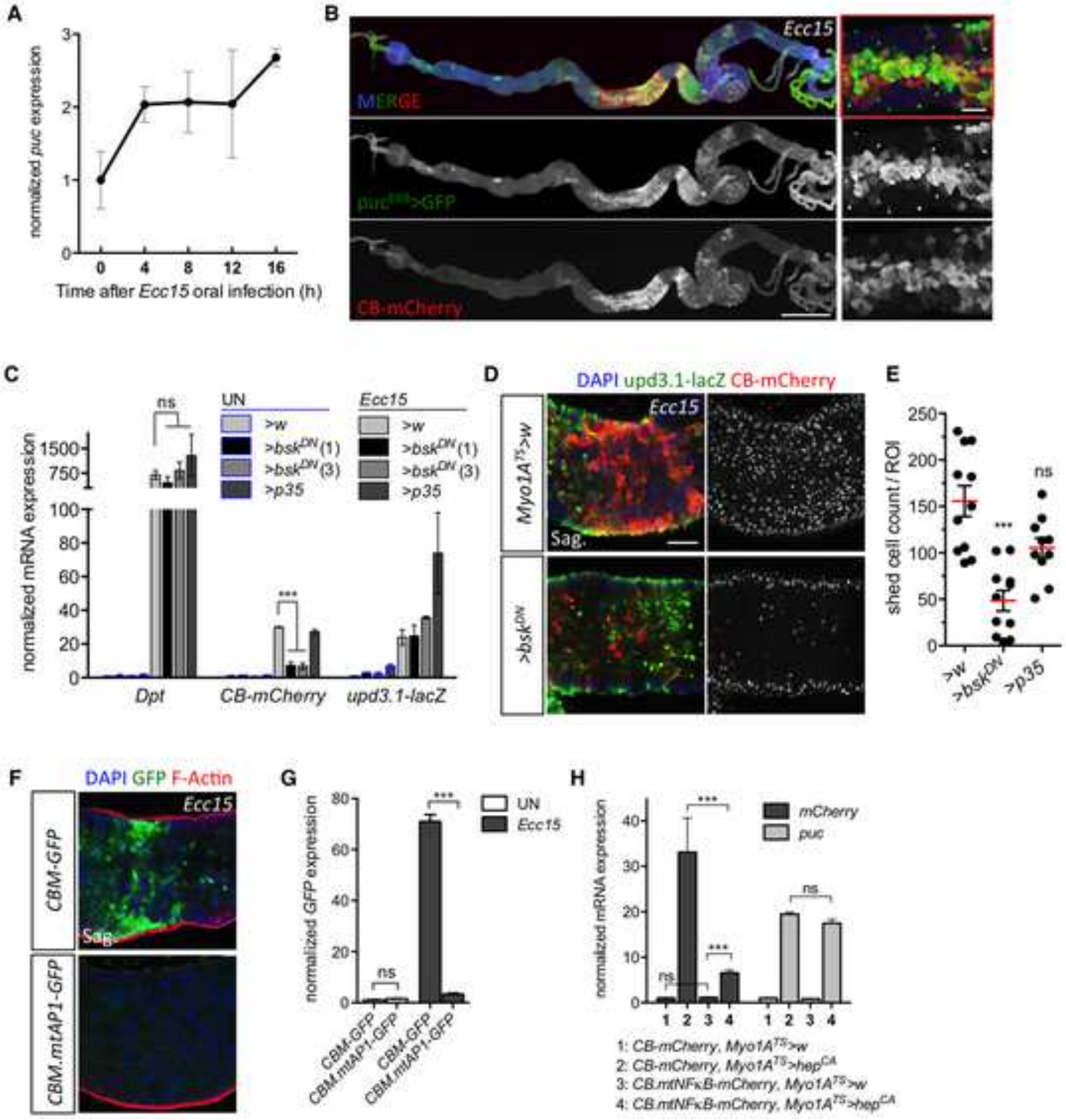

Figure 7

Click here to download Figure Fig 7-new-lzw.tif

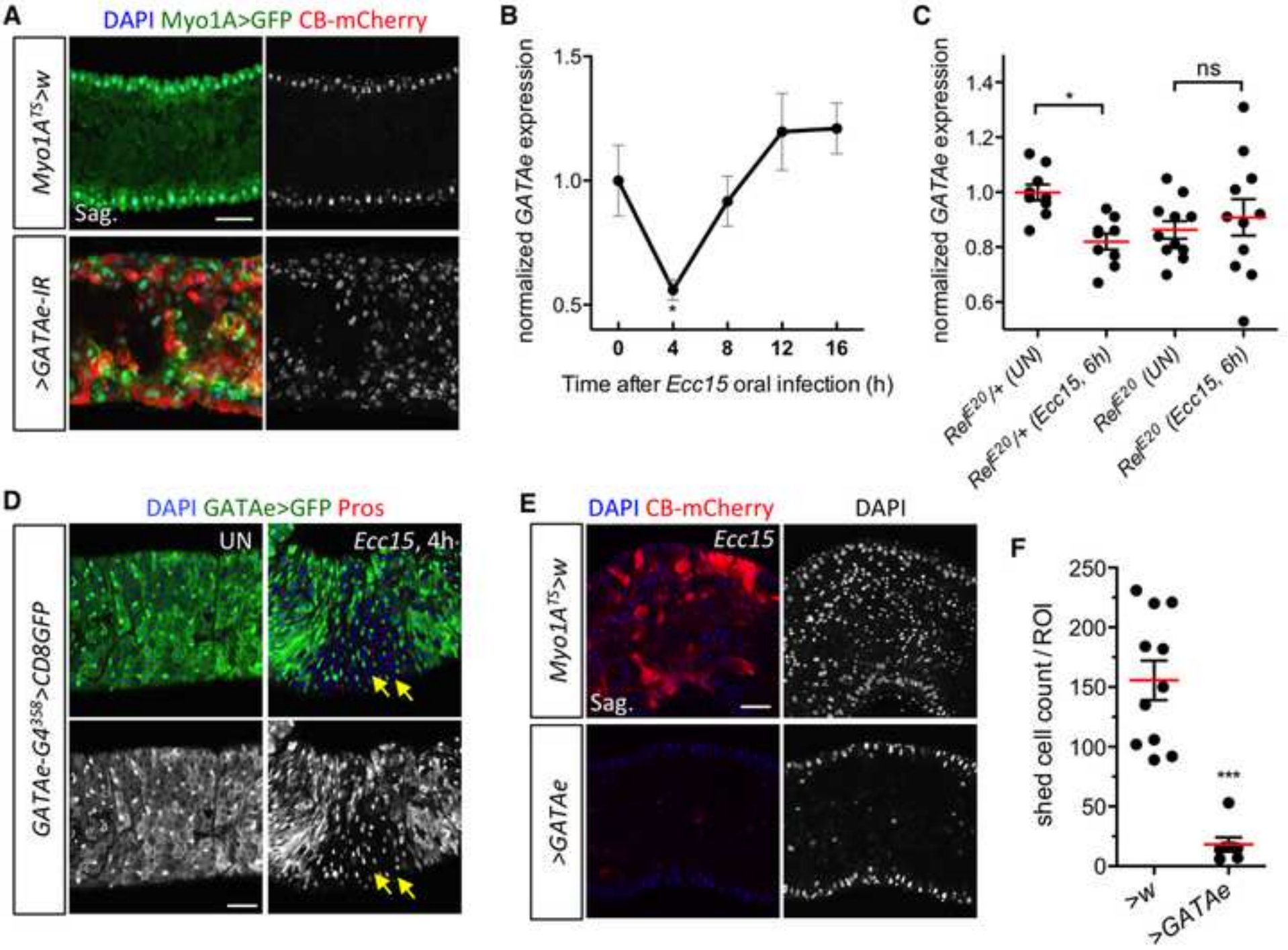

A

Fragment	Reporter	under basal conditions	upon *Ecc15* oral infection
1.9kb	Gal4, attP16	no expression	no expression
A	Gal4, attP16	midgut progenitors	midgut progenitors
B	Gal4, attP16	midgut progenitors	midgut progenitors
C	Gal4, attP16	no expression	induced in enterocytes
D	Gal4, attP16	a subset of EEs	a subset of EEs
CA	Gal4, attP16	no expression	no expression
CB (498bp)	Gal4, attP16 (II) mCherry, attP2 (III) GFP, attP40 (II)	no expression	induced in enterocytes
CBM (204bp)	GFP, attP16 (II) GFP, attP2 (III)	no expression	induced in enterocytes
CB-S1	GFP, attP2 (III)	no expression	no expression
CB-S2	GFP, attP2 (III)	no expression	no expression
CB-S3	GFP, attP2 (III)	no expression	no expression

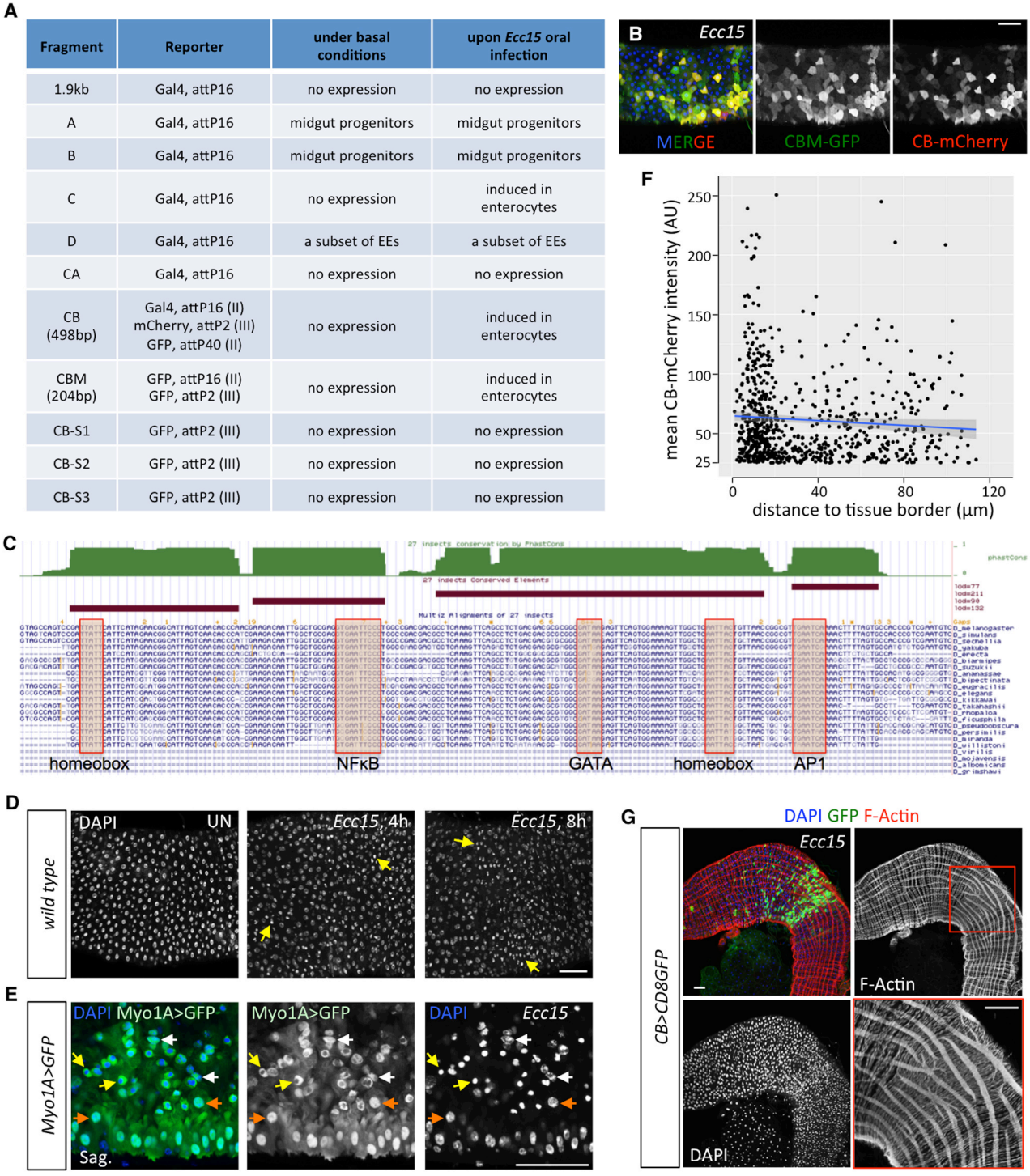

Figure S1. Identification of an infection-inducible enhancer fragment of *upd2*. Related to Figure 1.

(A) Summary of the reporter expression pattern in the midgut controlled by various cis-regulatory elements of *upd2*. Reporter types (*Gal4*, *mCherry* or *GFP*), transgene insertion sites in the *Drosophila* genome, and expression pattern of respective reporters both under basal conditions and upon *Ecc15* infection are listed. **(B)** Overlap of *CBM-GFP* and *CB-mCherry* reporters upon *Ecc15* infection (10hpi). **(C)** The sequences of the 204bp *CBM* enhancer with putative transcription factor binding sites. Conservation by phastCons scores was obtained from the UCSC genome browser. **(D)** Frontal view of the posterior midgut of wild-type flies at different time points post *Ecc15* infection (UN, 4 and 8hpi). Yellow arrows indicate ECs showing nuclear condensation. **(E)** Sagittal view of midgut epithelium from *Ecc15*-infected flies carrying *Myo1A>nlsGFP* (EC marker). Shedding ECs (orange arrows), shed ECs with ring or necklace-shaped chromatin condensation (white arrows) and shed ECs showing nuclear collapse and disassembly (yellow arrows) are indicated. **(F)** Quantitative measurements of *CB-mCherry* reporter levels and the distance of respective cell nuclei to the basal tissue border in *Ecc15*-infected gut. mCherry signal intensity below 25 is treated as background. Trend line and SEM are shown. n=13 guts. **(G)** Posterior midgut from *Ecc15*-infected *CB>CD8GFP* flies (10hpi). F-Actin is in red. Scale bars 50μm.

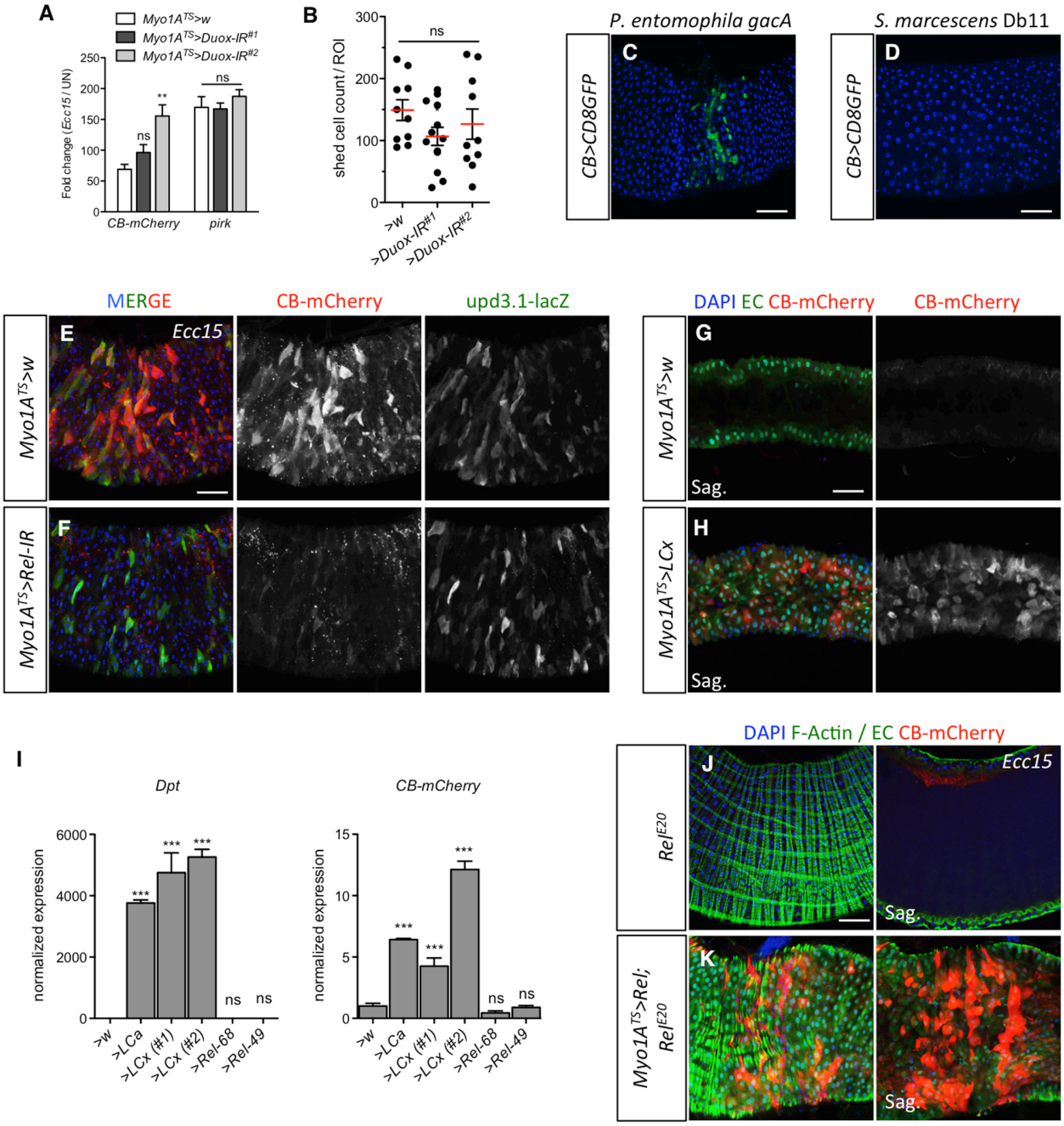

Figure S2. *CB* enhancer activity coincides with the levels of Imd signaling. Related to Figure 2.

(A) Expression of *mCherry* (*CB-mCherry*) and *pirk* (an Imd readout) as measured by qPCR in the midgut of flies RNAi of *Duox* in ECs using *Myo1A*^{TS} for 3 days. Results are presented as fold change of infected guts over unchallenged control. **(B)** Quantification of shed cells present in the gut lumen of *Ecc15*-infected control flies and flies depleting *Duox* using *Myo1A*^{TS} for 3 days. The image window was set to 320 µm x 320 µm. One dot represents one gut. **(C-D)** Induction of the *CB-Gal4/UAS-CD8GFP* reporter gene in the posterior midgut of flies challenged with *P. entomophila gacA* (C) or *S. marcescens* Db11 (D), at 10hpi. **(E-F)** Representative images of the posterior midgut of wild-type flies (upper panel, E) and flies with EC-specific depletion of *Relish* by RNAi (bottom panel, F) upon oral infection with *Ecc15* (12hpi). Note that the expression of *CB-mCherry* but not *upd3.1-lacZ* was affected by *Relish* depletion. **(G-H)** Sagittal view of the anterior midgut epithelium from wild-type flies (G) and *PGRP-LCx*-overexpressing flies (H) using *Myo1A*^{TS} (4 days at 29°C). **(I)** Expression of *Dpt* and *mCherry* (*CB-mCherry*) as measured by qPCR in the midgut of flies over-expressing various genes using *Myo1A*^{TS} for 2 days. **(J-K)** Expression of *CB-mcherry* in the posterior midgut of an *Ecc15*-infected (12hpi) *Relish* mutant fly (J) and a *Relish* mutant fly expressing a full-length form of *Relish* in ECs (K) with *Myo1A*^{TS}. Note that both EC shedding and *CB-mCherry* (in red) expression were restored when *Relish* was rescued. F-actin (in green) is shown for the upper panel and ECs (*Myo1A>GFP*, in green) for the bottom panel. Means and SEMs (n=3; ***p < 0.001, **p < 0.01, ns: p > 0.05; One-way ANOVA). Scale bars 50µm.

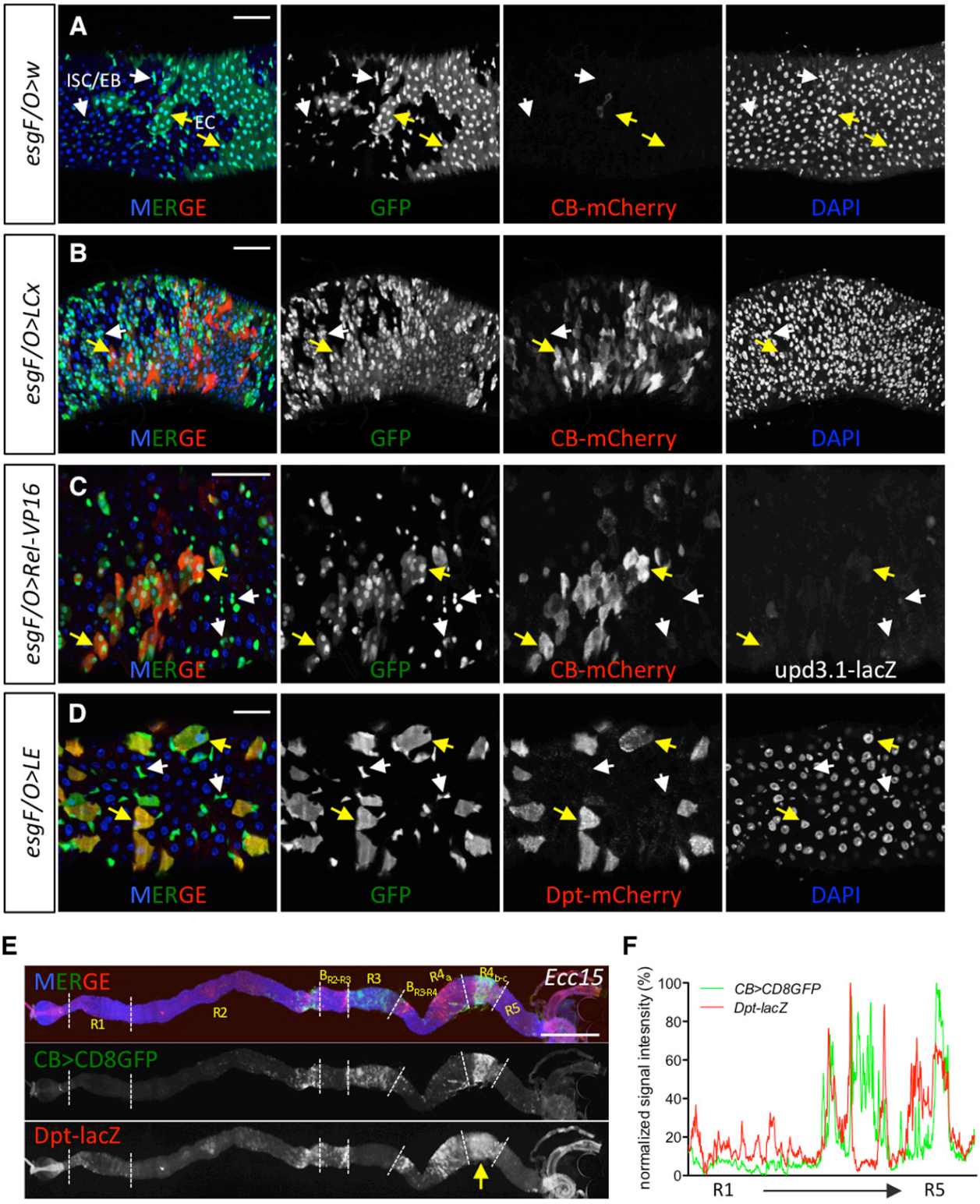

Figure S3. ECs are the only Imd-responsive cell type in the fly midgut. Related to Figure 3.

(A-D) Frontal view of midgut epithelium from wild-type flies and flies over-expressing various Imd pathway components (*PGRP-LCx*, *PGRP-LE* and *Rel-VP16*) using *esgF/O* for 4-7 days. White arrows indicate progenitors; yellow arrows indicate newly generated ECs. Only GFP-marked cells over-express UAS-linked genes. ECs can be identified based on their large nuclei size and round cell shape. Expressing *PGRP-LCx*, *Rel-VP16* and *PGRP-LE* activated both *CB-mCherry* and *Dpt-mCherry* only in ECs in a cell-autonomous manner. No expression of these reporters was found in the GFP-marked progenitors suggesting that these reporter genes are only induced in ECs. Scale bars 50µm. **(E-F)** Expression of *CB* and *Dpt* reporters (*CB>CD8GFP / Dpt-lacZ*) in the midgut of *Ecc15*-infected flies (E) and quantification of respective reporter intensity profile along the length of the midgut (F). The two reporters were expressed in ECs of different gut regions. Arrow in E indicates non-specific staining of β-Gal due to massive EC shedding in this region. Scale bar in E 500µm.

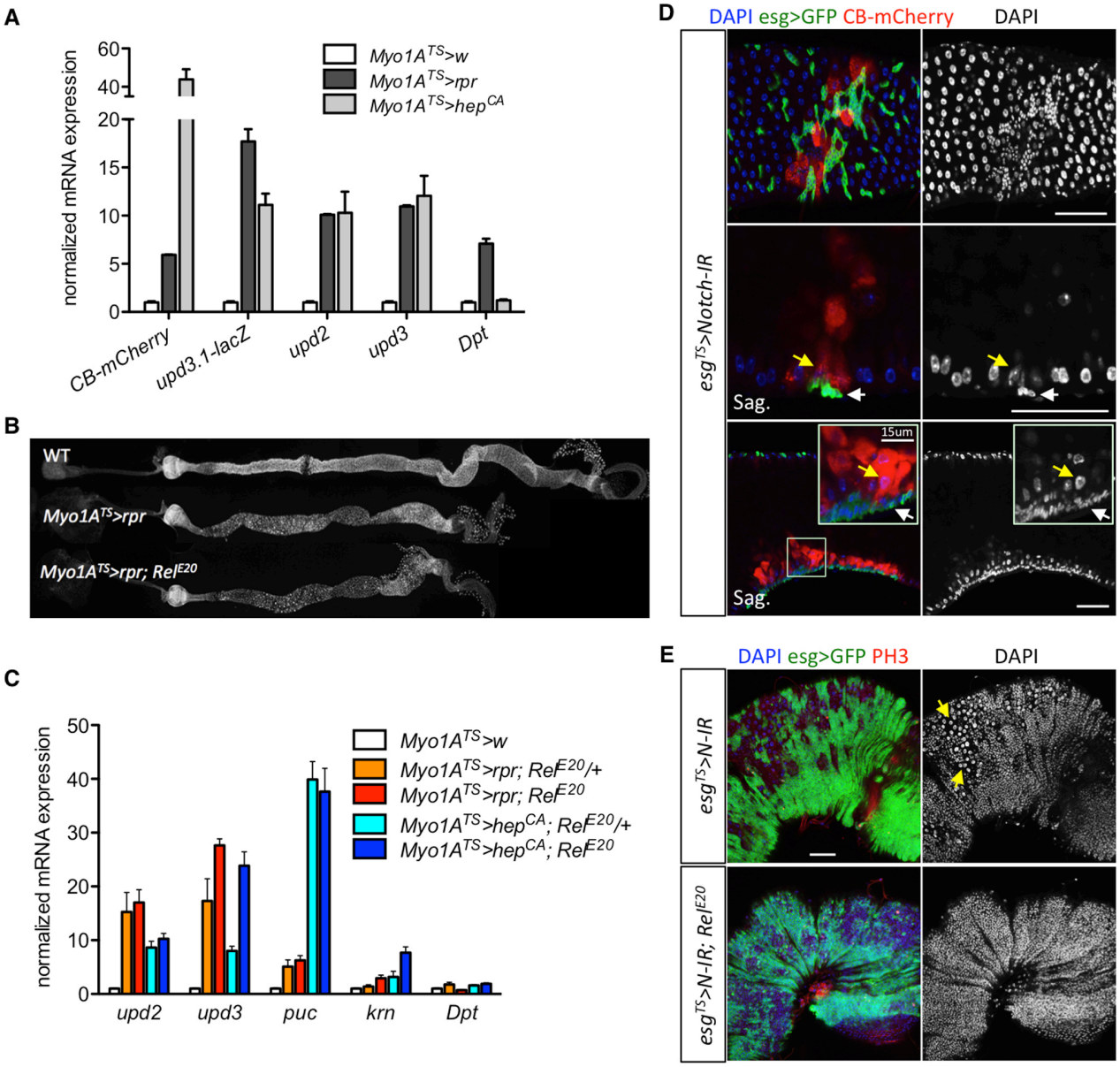

Figure S4. *Relish* is not required for other forms of EC death. Related to Figure 5.

(A) Expression of various reporter genes or endogenous genes in the midgut of flies with EC-specific expression of *reaper (rpr)* or hep^{CA} for 15 hours as monitored by qPCR. **(B)** Over-expressing the pro-apoptotic gene *reaper* in ECs induced cell death and midgut shortening in both wild-type and *Relish* mutant flies. *reaper* was over-expressed for 36 hours at 29°C. **(C)** Expression of *upds* and *Keren* but not *Dpt* were induced upon expression of *reaper* or hep^{CA} in ECs. The induction of *upds* and *Keren* was not blocked in Rel^{E20} flies. **(D)** *CB-mCherry* reporter activation in ECs at the vicinity of *Notch*-deficient ISC tumors. *Notch* was silenced by RNAi in the midgut progenitors using esg^{TS} for 4 days. Progenitors are marked with *esg>GFP* (green). Yellow arrows indicate shedding ECs; white arrows indicate progenitor cells. **(E)** Representative images of posterior midgut bearing ISC tumors in wild-type (upper panel) or *Relish* mutant background (bottom panel). Arrows indicate remaining ECs that had not been eliminated by the ISC tumors. Means and SEMs (n=3). Scale bars 50μm.

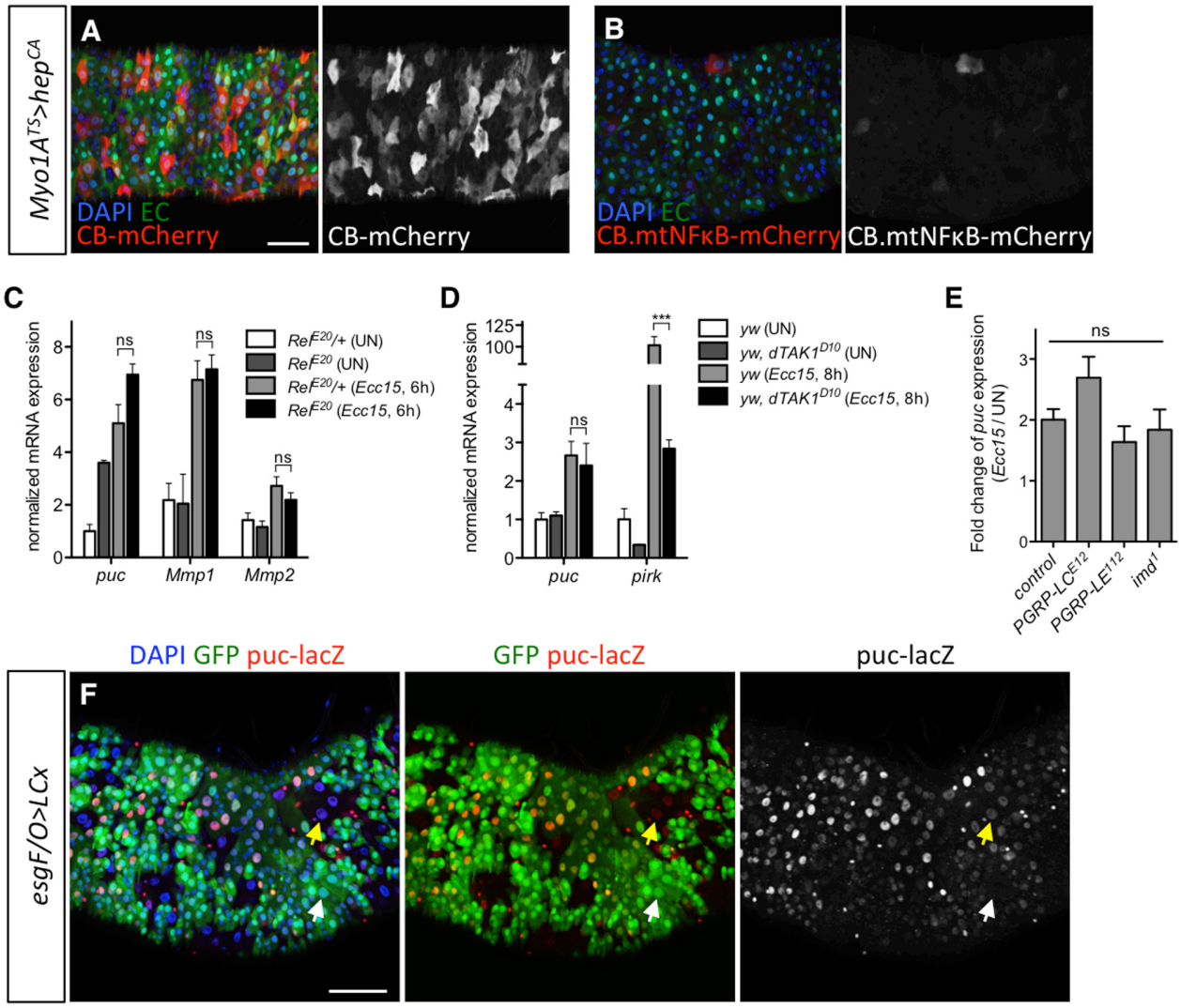

Figure S5. JNK activation upon infection is independent of the Imd pathway. Related to Figure 6.

(A-B) Representative images showing activation of *CB-mCherry* (A) and *CB.mtNFκB-mCherry* (B) reporters in the midgut upon EC-specific over-expression of hep^{CA} for 15 hours. **(C)** Expression of JNK target genes (*puc, Mmp1* and *Mmp2*) in control (Rel^{E20}/+) and Rel^{E20} mutants under basal conditions (UN) and upon infection (*Ecc15*, 6hpi). **(D)** Expression of the JNK target gene *puc* and the Imd-target gene *pirk* in wild-type control (*yw*) and *yw, dTAK1* mutant under basal conditions (UN) and upon infection (*Ecc15*, 8hpi). **(E)** Expression of *puc* as measured by qPCR in the midgut of flies with indicated genotype. Results are presented as fold change of infected guts over unchallenged control. **(F)** Midgut with GFP-labeled clones over-expressing *PGRP-LCx* via *esgF/O* for 5 days. *puc-lacZ* expression was detected by immunostaining. The white arrow indicates a GFP^{+} EC that does not express *puc-lacZ* reporter, while the yellow arrow indicates a $GFP^{negative}$ EC that expresses *puc-lacZ*. Means and SEMs (n>3; ***p < 0.001, ns: p > 0.05; One-way ANOVA). Scale bars 50µm.

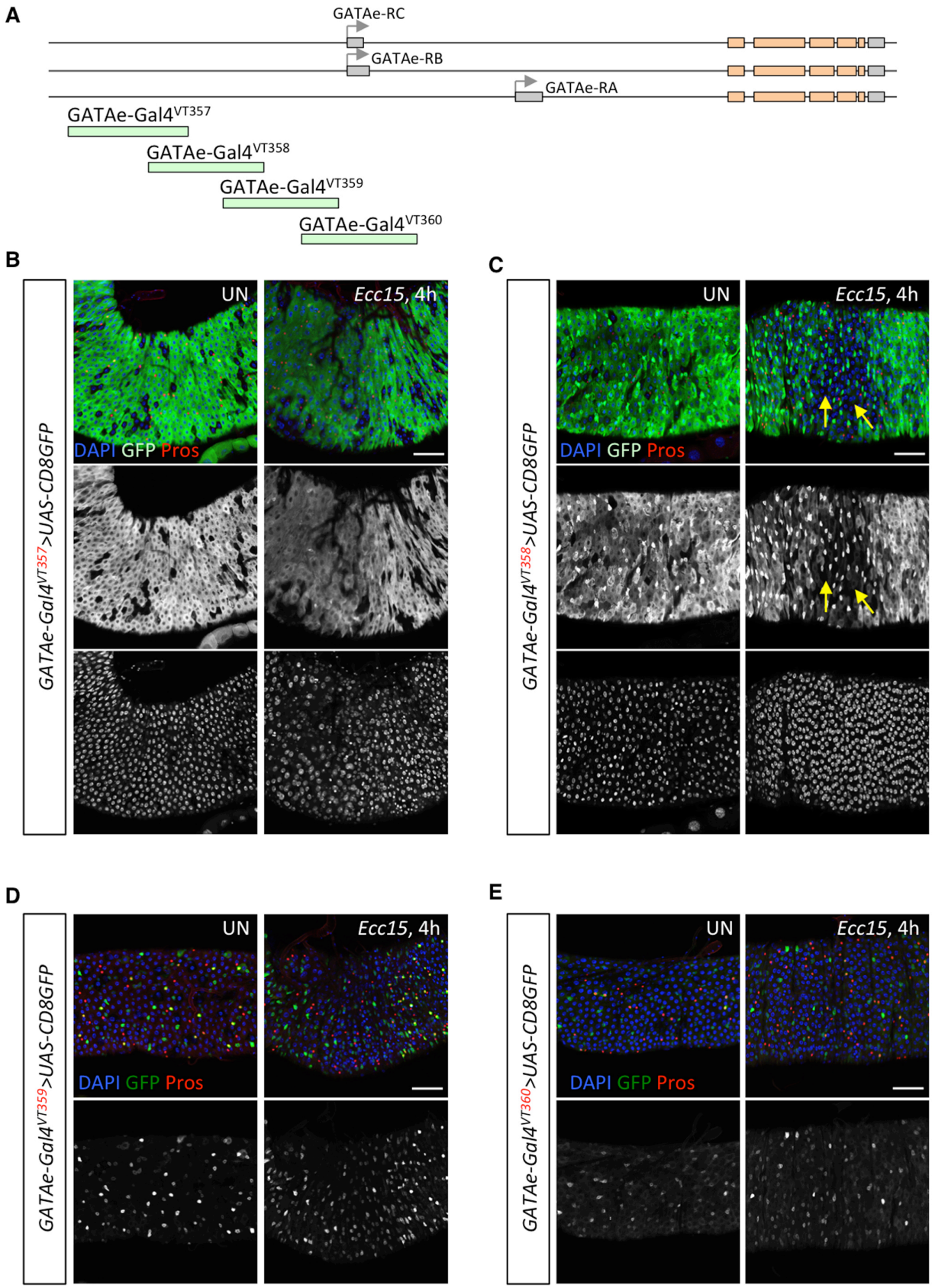

Figure S6. Analysis of the enhancer activity of *GATAe* cis-regulatory elements. Related to Figure 7.

(A) Schematic representation of the *GATAe* cis-regulatory sequence analyzed in the present study (lines 357-360). **(B-E)** Expression pattern of various *GATAe-Gal4/UAS-CD8GFP* reporters in the posterior midgut of flies either unchallenged (UN) or orally infected with *Ecc15* (4hpi). The line 357 marks ECs; line 358 marks both ECs and midgut progenitors; both lines 359 and 360 mark midgut progenitors and a subset of EEs. The absence of GFP signal in some ECs in the region where massive EC shedding will take place is indicated with arrows in C. Pros staining shown in red marks EEs. Scale bars 50µm.

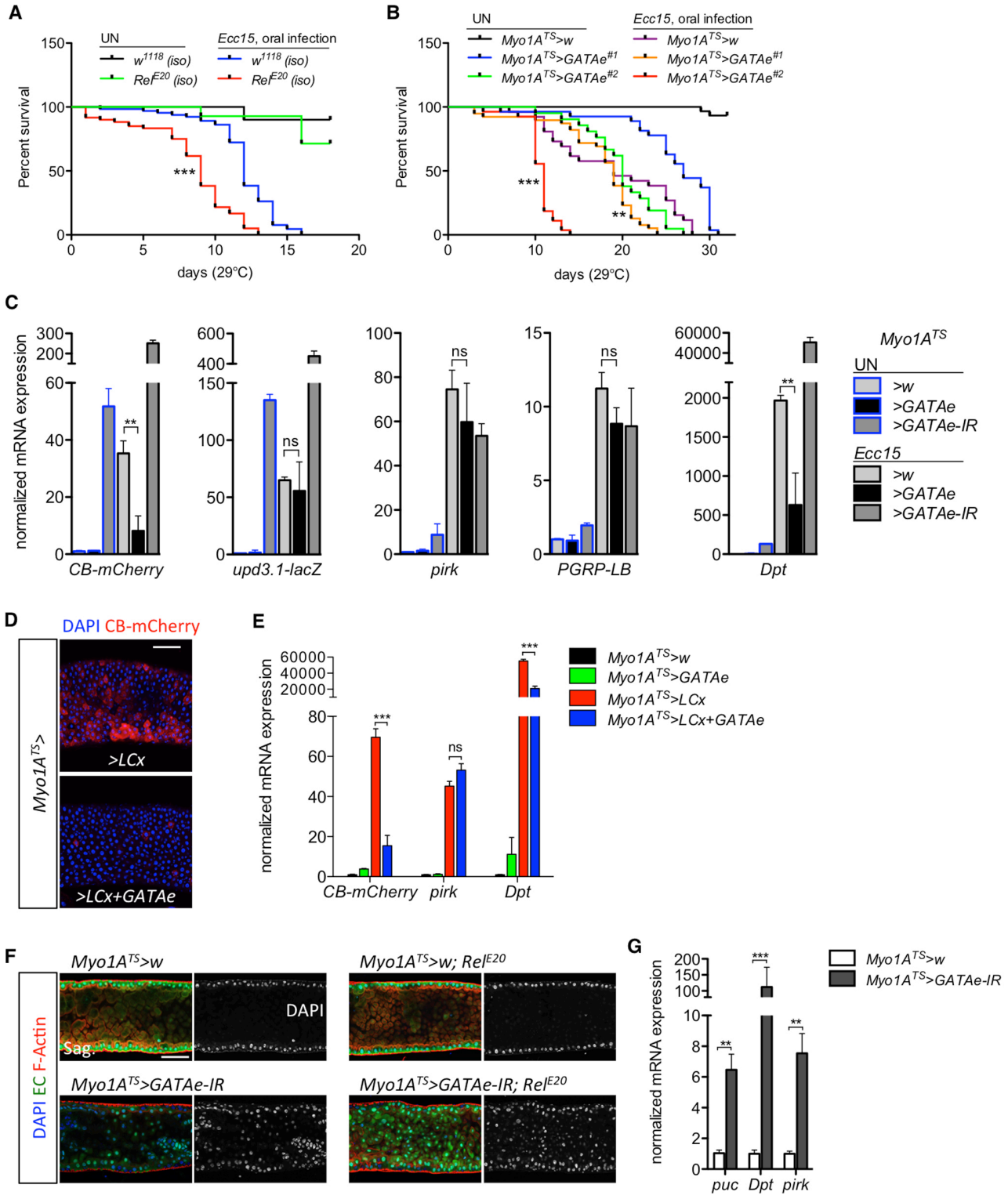

Figure S7. GATAe is essential for EC survival. Related to Figure 7.

(A) Survival analysis of isogenic wild-type and Rel^{E20} female flies upon infection with *Ecc15*. (**B**) Survival of wild-type flies and flies over-expressing *GATAe* in ECs upon *Ecc15* infection. ***p < 0.0001, **p < 0.001; Log-rank test. **(C)** qPCR analysis of the expression of the indicated reporters or genes in the midgut of unchallenged or infected (*Ecc15*, 16hpi) flies with EC-specific depletion (*>GATAe-IR*) or over-expression (*>GATAe*) of *GATAe* for 2-3 days. Means and SEMs (n=4; **p < 0.01, ns: p > 0.05; One-way ANOVA). **(D)** Immunofluorescence showing the activation of *CB-mCherry* reporter upon over-expression of *PGRP-LCx* alone or in combination with *GATAe* with $Myo1A^{TS}$ for 4 days. **(E)** qPCR quantification of *mCherry*, *pirk* and *Dpt* expression in the midgut of indicated flies. Means and SEMs (n=3; ***p < 0.001, **p < 0.01, *p < 0.05, ns: p > 0.05; One-way ANOVA). **(F)** Sagittal view of midguts from indicated flies shifted to 29°C for 3-4 days. EC shedding induced upon RNAi of *GATAe* in ECs was not suppressed in Rel^{E20} flies. **(G)** qPCR quantification of gene expression (*puc, Dpt* and *pirk*) in the midgut of wild-type flies and flies with a specific depletion of *GATAe* in ECs. Means and SEMs (n=3; ***p < 0.001, **p < 0.01; Student's *t* test). Scale bars 50µm.